UNIVERSITAT POLITÈCNICA DE CATALUNYA
BARCELONATECH
Departament d'Enginyeria Civil i Ambiental

CIMNE

Exploring air migration in argillaceous formations: experimental results and numerical modelling

Enrique Romero & Laura Gonzalez-Blanco

IV International workshop
Modern Trends in Geomechanics
Assisi, May 16 -18 2016

Session 11: Experimental Geomechanics

18 May 2016: 10:00 – 10:30

Outline of the presentation

1. Preliminary insight into gas (air) transport

2. Experimental study

- Material, equipment and protocols
- Typical experimental results
- Interpretation of results

3. Numerical modelling (incorporating experimental information)

4. Concluding remarks

Understanding gas transport process is an important issue in the assessment of radioactive waste repository performance and other energy geotechnics related fields

Anaerobic corrosion of iron contained in the canister overpacks (largest source and production of hydrogen). Gas pressure build-up may cause the failure of the EBS and the possible release of radionuclides into environment (long-term behaviour)

Gas transport mechanisms (all of them may be present to a certain degree):

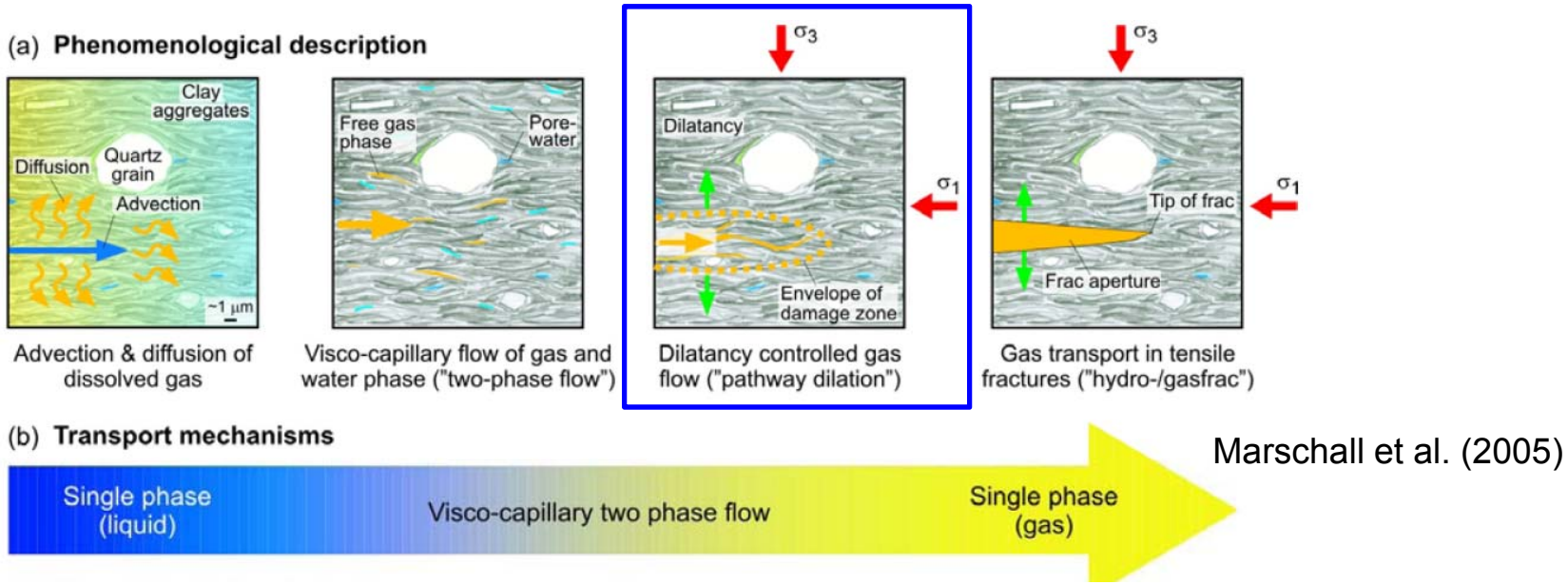

Marschall et al. (2005)

- Flow properties of matrix affected by mechanical effects (porosity changes due to compressibility of skeleton)
- Enhancement through opening of pressure-dependent discontinuities (fracturing of porous medium: fracture opening or fracture formation)
- Intrinsic permeability and water retention properties affected by aperture variations

Some preliminary issues

Linking gas migration process and pathway development to the stress-strain response during injection remains challenging, particularly from an experimental point of view

- The gas pressurisation process at constant total stress acts as an unloading stage, which may induce expansion and degradation (opening of bedding planes / fissures) on the clay and that could have important consequences on gas transport properties

- To analyse the changes in the pore / fissure network of the clay due to gas injection process (opening of bedding planes / fissures)

- To study the volume change behaviour during gas injection and gas dissipation stages and their impact on gas permeability (stress state and stress history, orientation of rock discontinuities, degradation of the material, …)

- Simple concepts but no so simple tests, in which not all the information is usually provided by experiments. Need for coupled modelling to complement the information not provided by measurements (‘boundary value tests’)

Preliminary insight. Degradation / fissuring issues before air permeability tests

Tertiary (Eocene) Lilla claystone (Spain).
Rock matrix (clayey fraction + large size minerals)

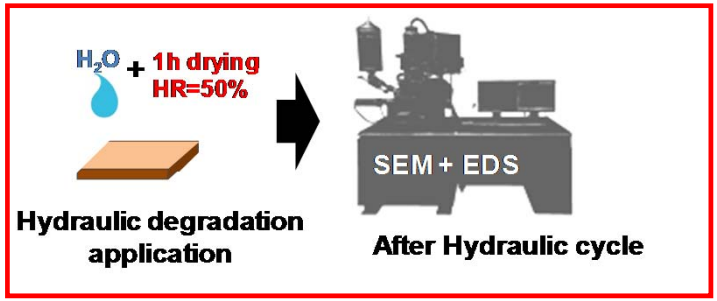

Pineda, Alonso & Romero (2014). Géotechnique

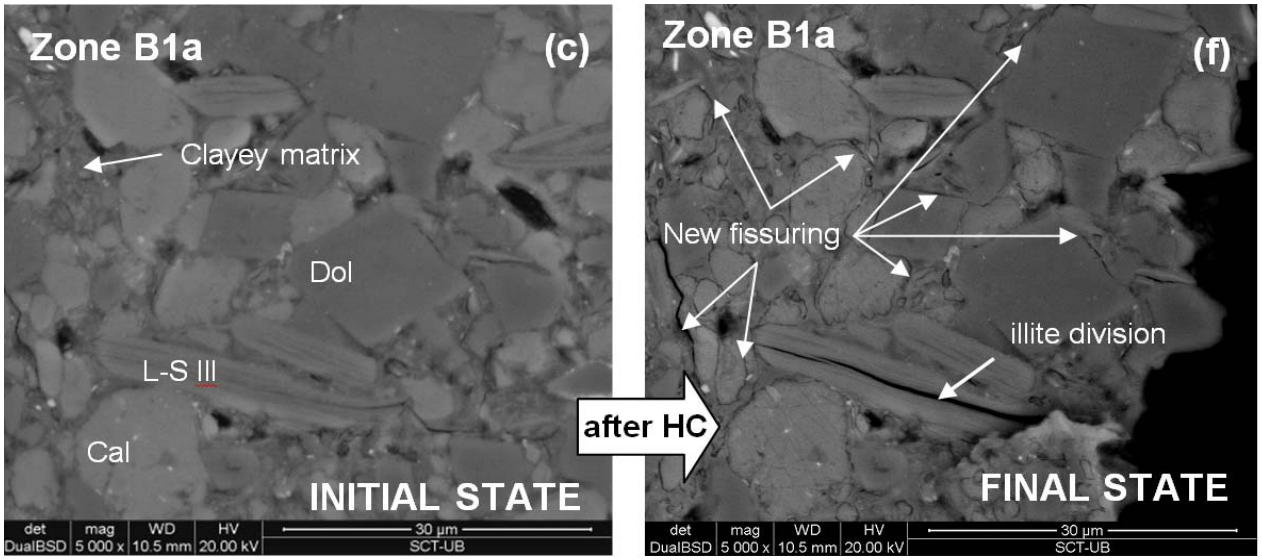

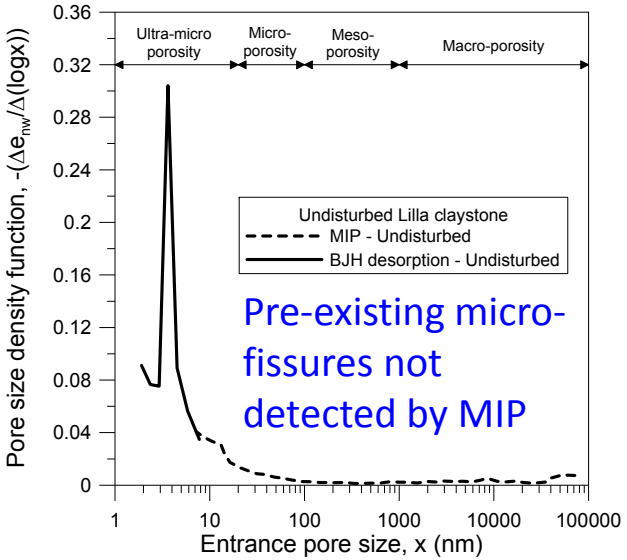

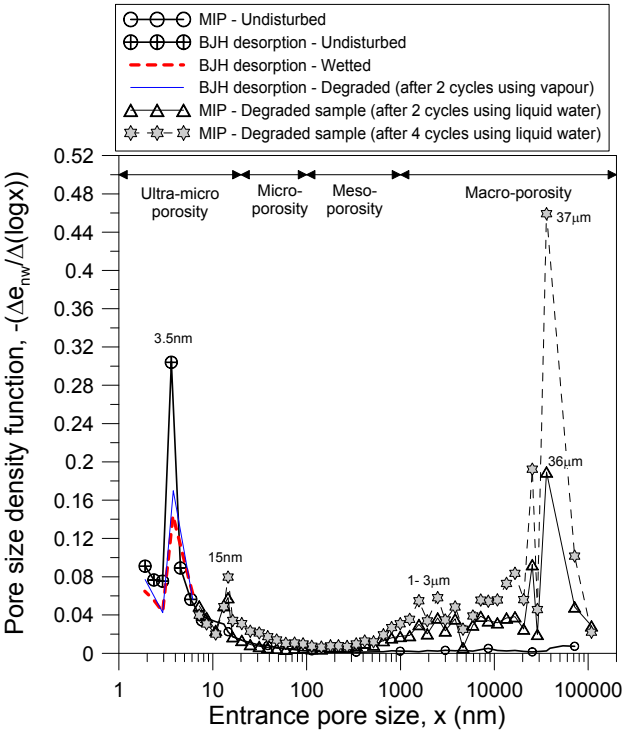

Micro-fissuring developed mainly at the interfaces between the clayey matrix and the large-size minerals (rigid inclusions)

Preliminary insight. Degradation / fissuring issues before air permeability tests

RH cycles (ventilation)

$$\left[(1-D)-r\right]=\left[(1-D_0)-r\right]\exp^{-\chi\left|\varepsilon_v^{damage}\right|}$$

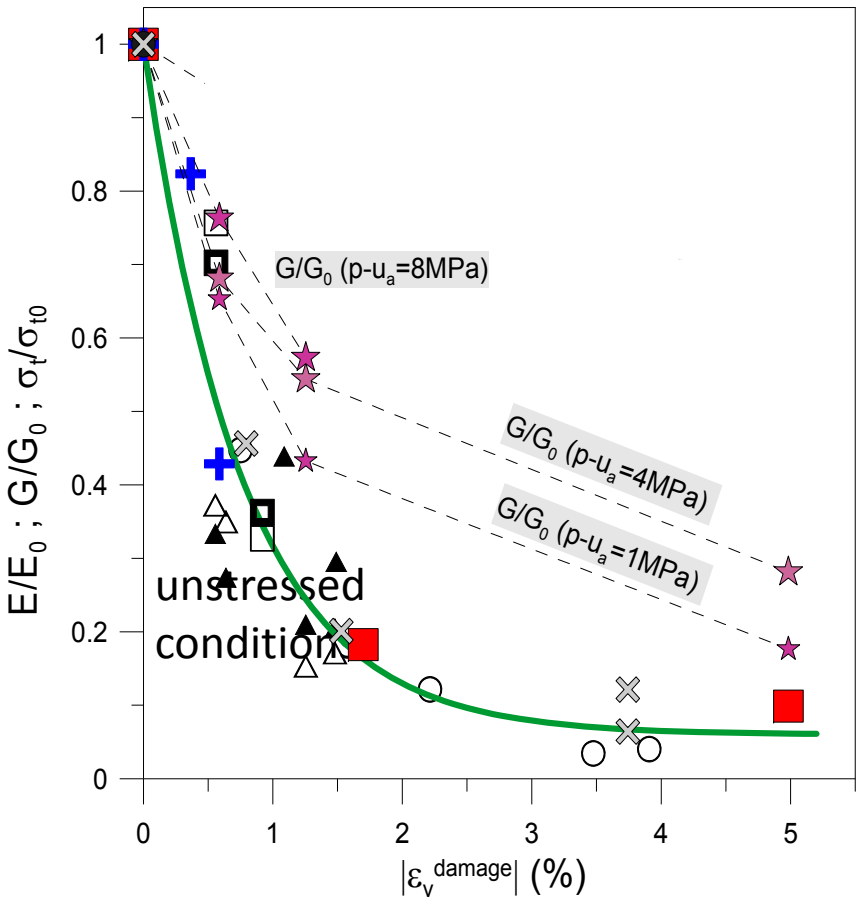

D law for both rock stiffness (Young and shear moduli) and tensile strength

Pineda, Alonso & Romero (2014). Géotechnique

Pressure decay method (RH = 50%)

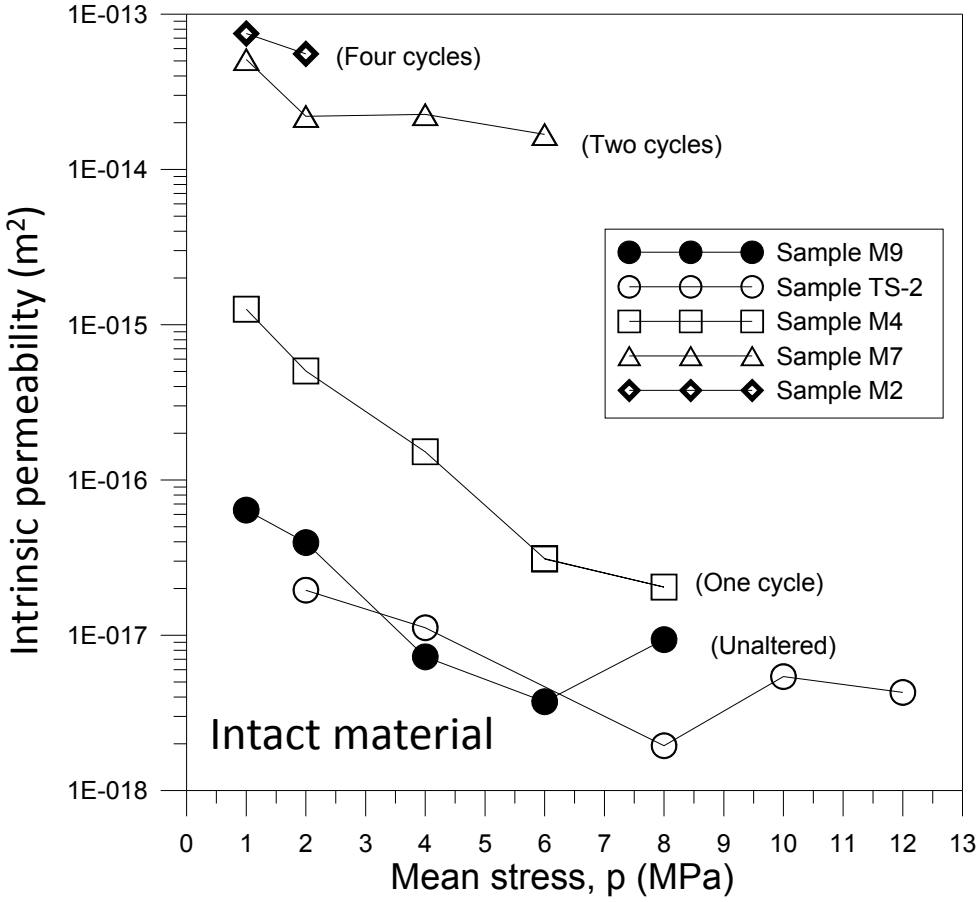

Pineda et al. (2014). Geot. Testing Journal

Preliminary insight. Degradation / fissuring issues before air permeability tests

Pressure decay method (RH = 50%)

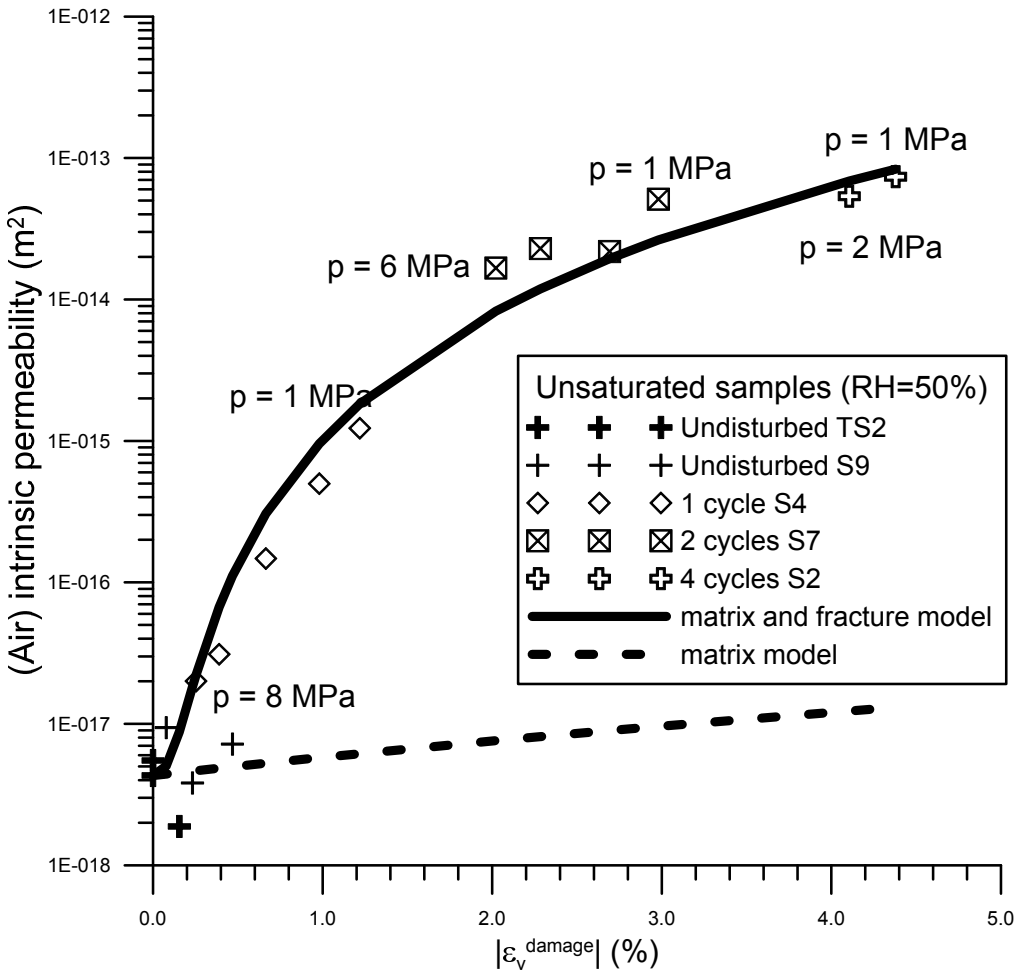

RH cycles at low stresses

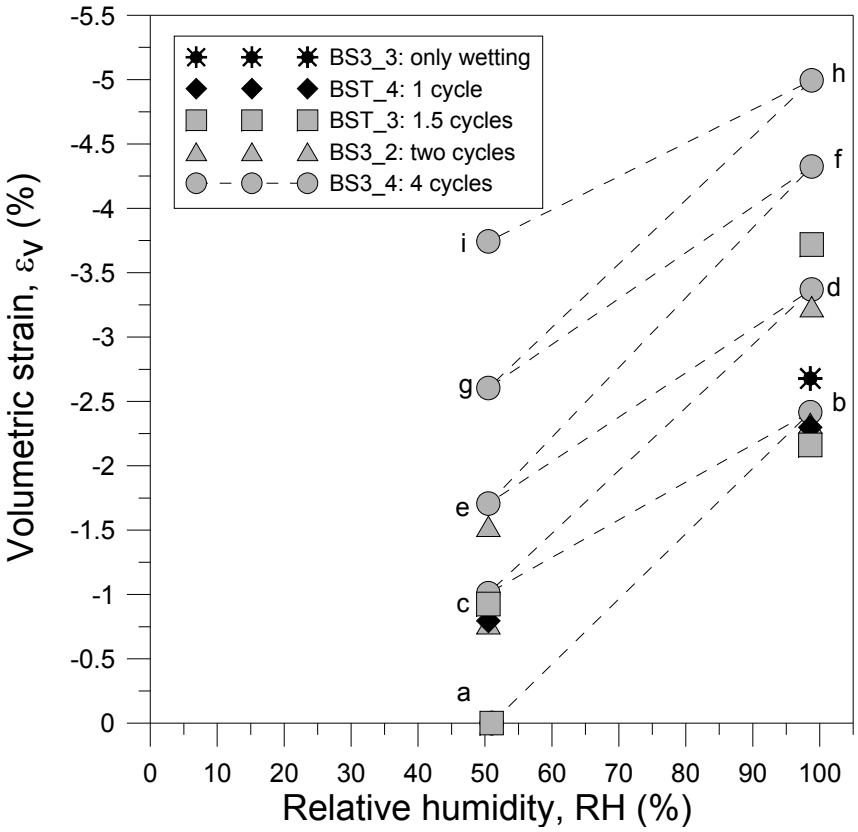

Pineda (2012)

$$k_{matrix} = k_0 \frac{\phi^3}{(1-\phi)^2} \frac{(1-\phi_0)^2}{\phi_0^3} \qquad k_{sample} = k_{matrix} + \frac{(b_0 + \Delta b)^3}{12a} \qquad \Delta b = a\Delta\varepsilon$$

Material 1: Boom Clay (BC), medium-deep plastic clay formation

Retrieved at a depth of 223 m and two different orientations (Hades, Mol, Belgium)

Main properties / Initial conditions	Values
Density of soils ρ_s (Mg/m^3)	2.67
Plastic limit w_P (%)	29
Liquid limit w_L (%)	67
Dominant entrance pore size from mercury intrusion porosimetry (nm)	65
Air-entry value from dominant entrance pore size (MPa)	4.8
Dry density ρ_d (Mg/m^3)	1.66-1.69
Void ratio e	0.58-0.61
Water content w (%)	22.6-24.0
Degree of saturation S_r	close to 1
Total suction ψ (MPa)	2.45

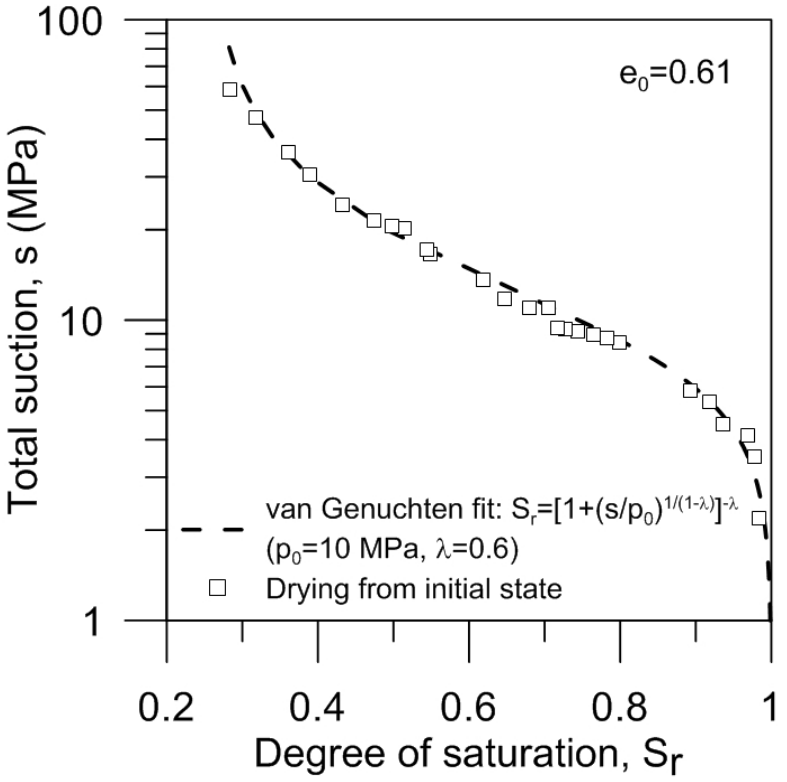

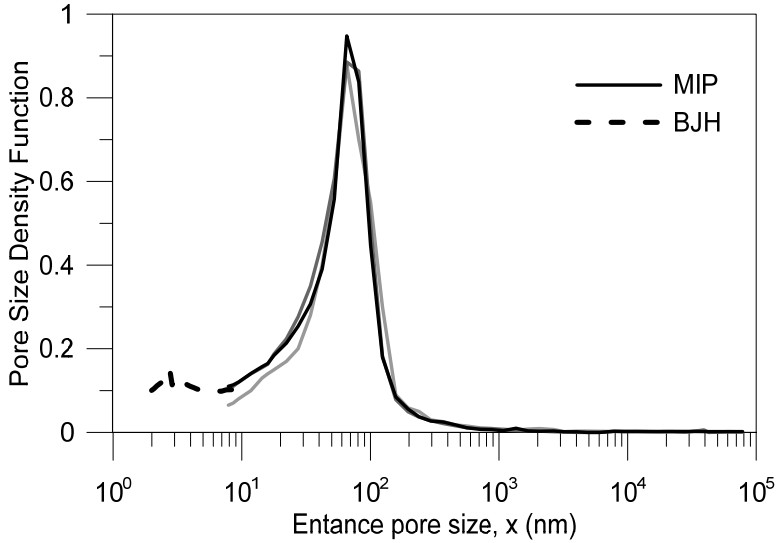

Materials 2 and 3: Opalinus Clay (OPA) and 'Brauner Dogger' (BD), deep indurated clay

Retrieved from the geothermal well Schlattingen-1 (Switzerland) at 880 and 936 m (OPA) and at 777 and 782 m (BD)

Formation	Brauner Dogger		Opalinus Clay	
Depth (m)	777	782	880	936
Density (Mg/m^3)	2.51	2.55	2.53	2.53
Water content (%)	4.34 – 5.43	4.78	4.30 - 4.70	4.79
Density of solids (Mg/m^3)	2.69	2.69	2.69	2.69
Void ratio, e	0.116 – 0.130	0.090	0.107 – 0.112	0.110
Porosity, n	0.104 – 0.115	0.080	0.097 – 0.101	0.100
Degree of saturation, S_r	1.0	0.95 - 1.0	1.0	0.98 - 1.0
Dominant pore mode from MIP (nm)	20	22	16	< 8
Air-entry value from MIP (MPa)	14	13	18	> 36
Liquid limit, w_L (%)	28	24	-	29
Plastic limit, w_P (%)	18	17	-	18

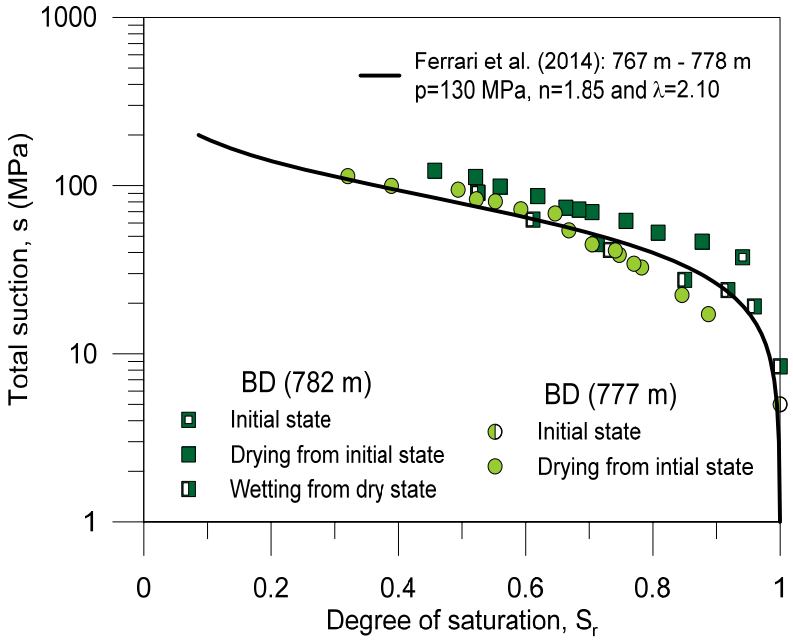

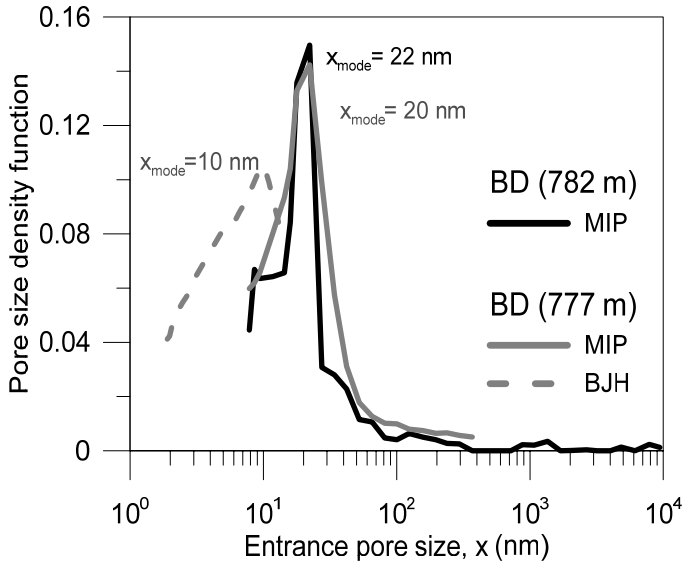

Water permeability

BC (223 m)
Flow ⊥ bedding

BC (223 m)
Flow // bedding

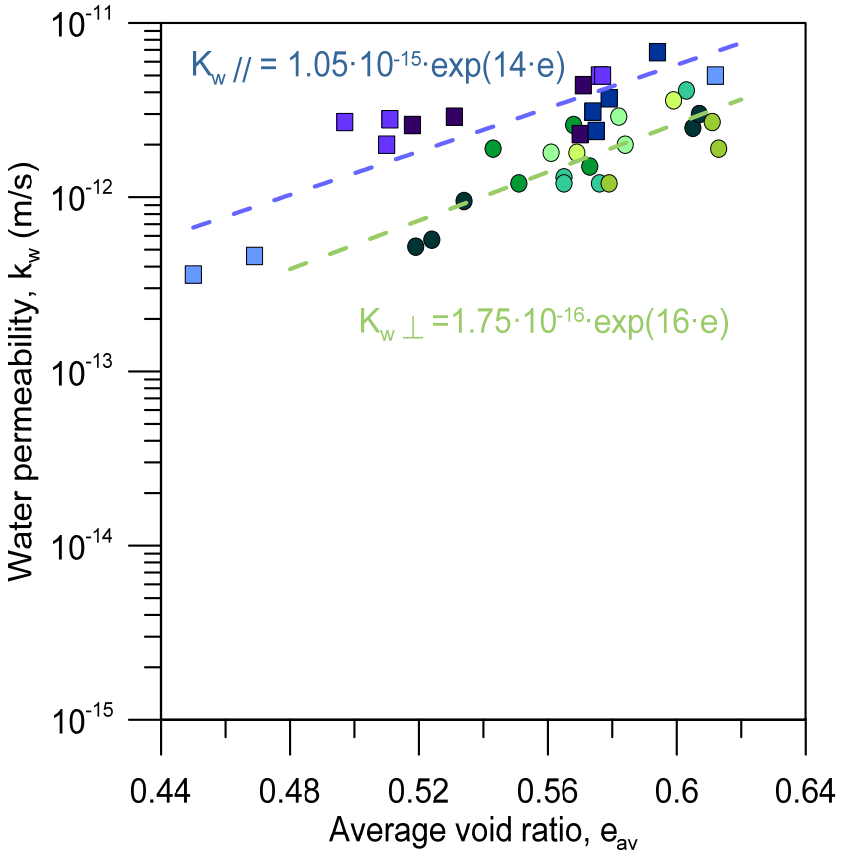

'Brauner Dogger' samples
BD (782 m)
BD (777 m)
BD (767 -778 m) (Ferrari & Laloui, 2012)

Opalinus Clay samples
OPA (936 m)
OPA (880 m)
OPA (Mont Terri URL)(Ferrari & Laloui, 2012)

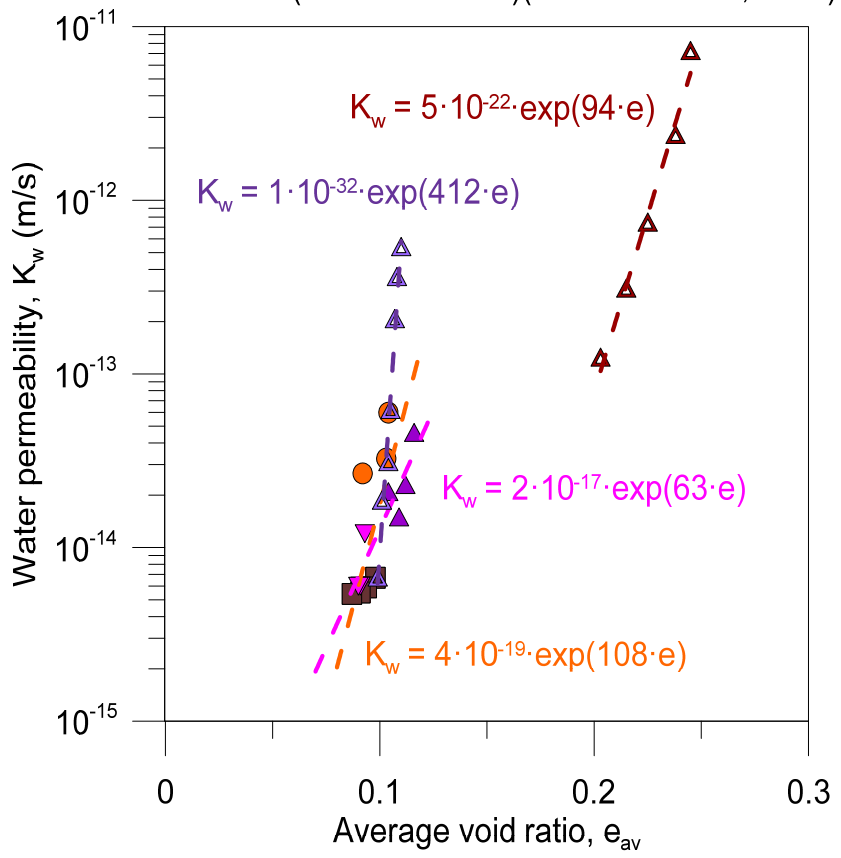

Equipment for air injection tests

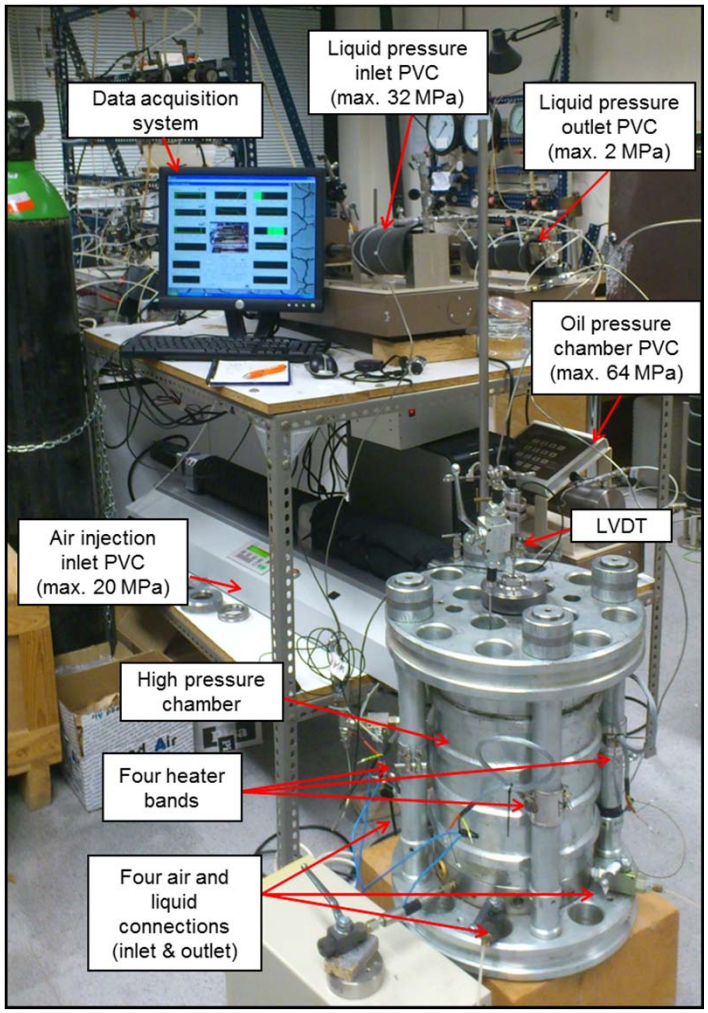

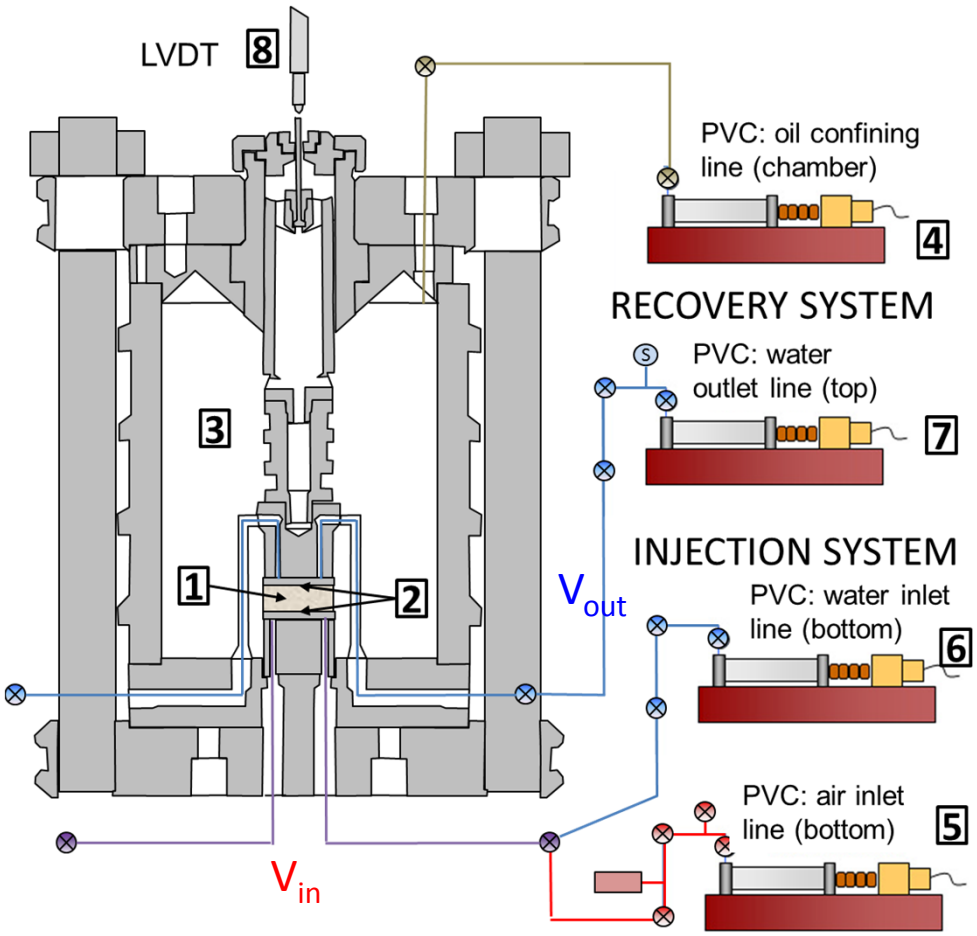

Triaxial/isotropic cell
(25 mm in height, 50 mm in diameter)

Typical test protocol: OPA and BD air injection tests

1st Stage: **Pre-conditioning**. Fast isotropic loading up to 10 MPa at constant water content (suction changes)

2nd Stage: **Flooding**. Contact with Artificial Pore Water (APW) and water permeability determination ($u_{w\ in}$=2 MPa; $u_{w\ out}$=0.5 MPa).

3rd Stage: Isotropic **loading** up to 15 MPa (and 19 MPa)

4th Stage: **Drainage** of the bottom cap. Fast replacement of water by air

5th Stage: Fast (r=100mL/min) or slow (r=2mL/min) or very slow (r=0.04mL/min) **air injection, shut-off and dissipation**

6th Stage: Fast undrained **unloading**

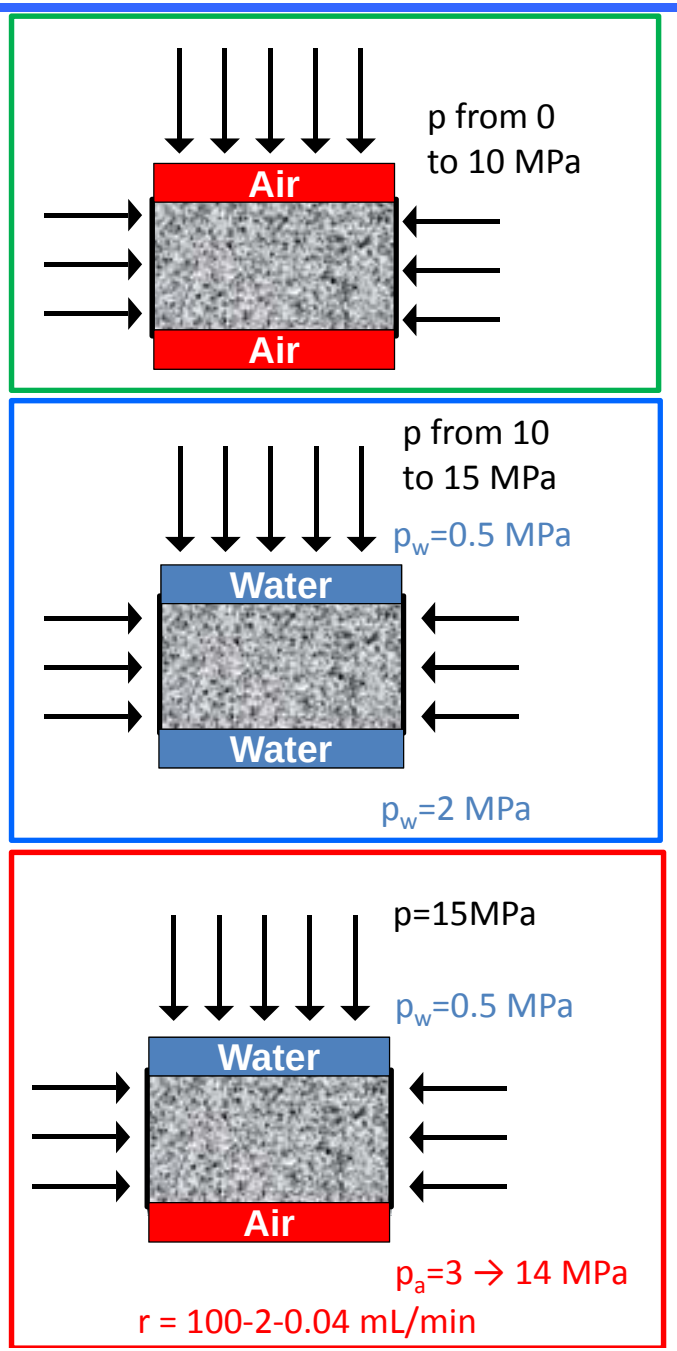

Typical air injection tests (BC)

Constant vertical stress σ_v= 6 MPa
(oedometer conditions)

A→B: Air injection at constant volume rate (r) from 0.5 MPa to 4 MPa (below AEV)

B: Shut-off of the injection system

B→C: Air dissipation at constant injection volume (at the injection point)

Gonzalez-Blanco et al. (2016)

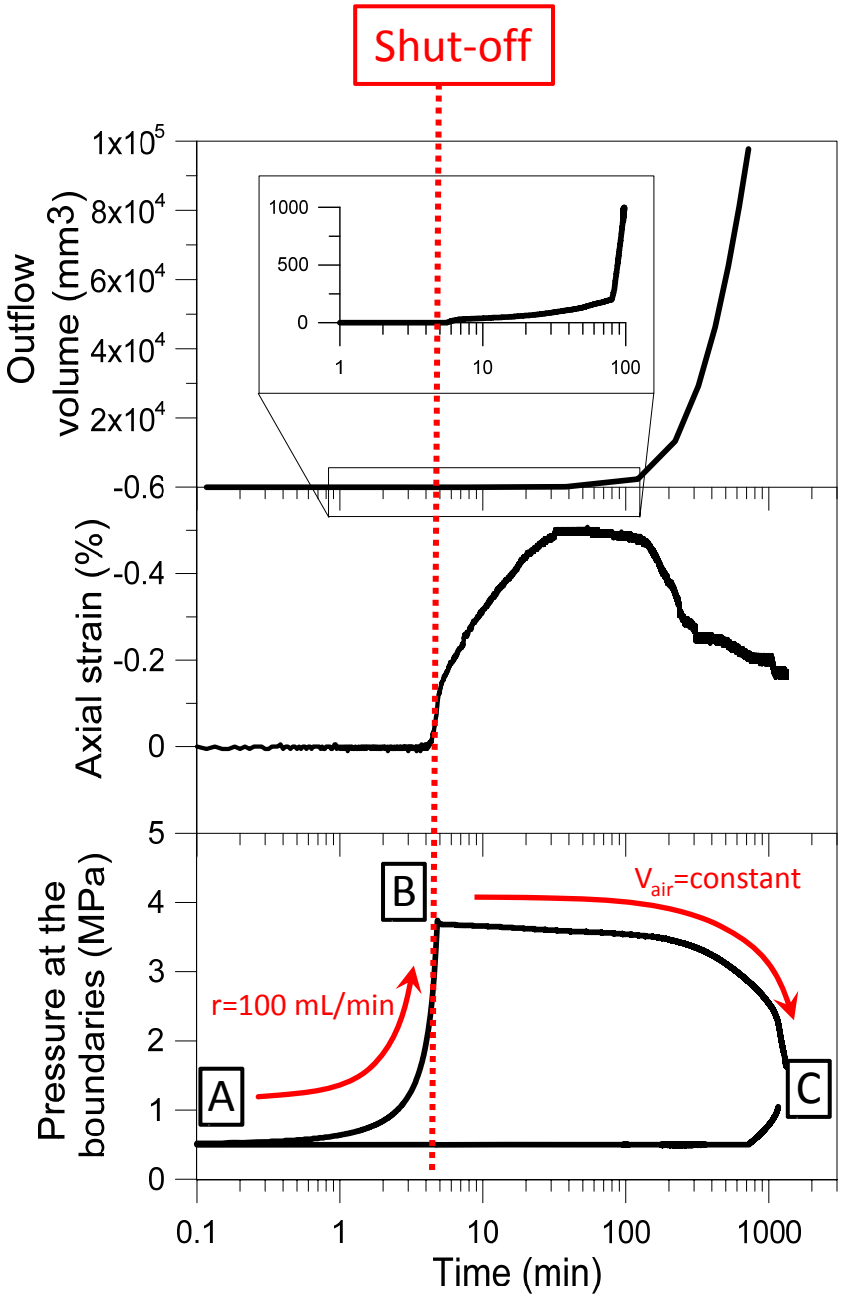

Results of fast air injection tests: BC (oedometer conditions). Below AEV

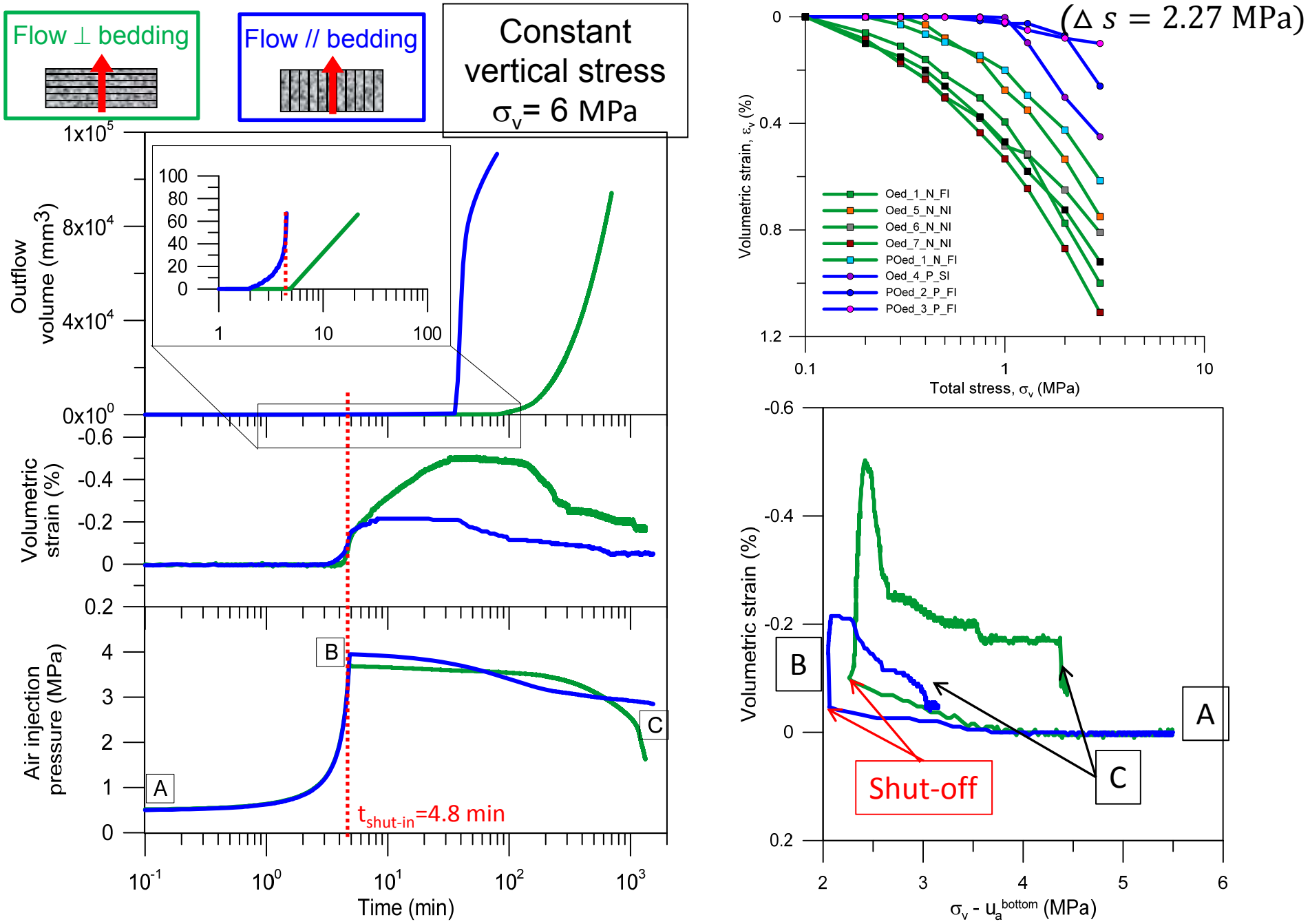

Results of fast air injection tests on OPA and BD. Below AEV

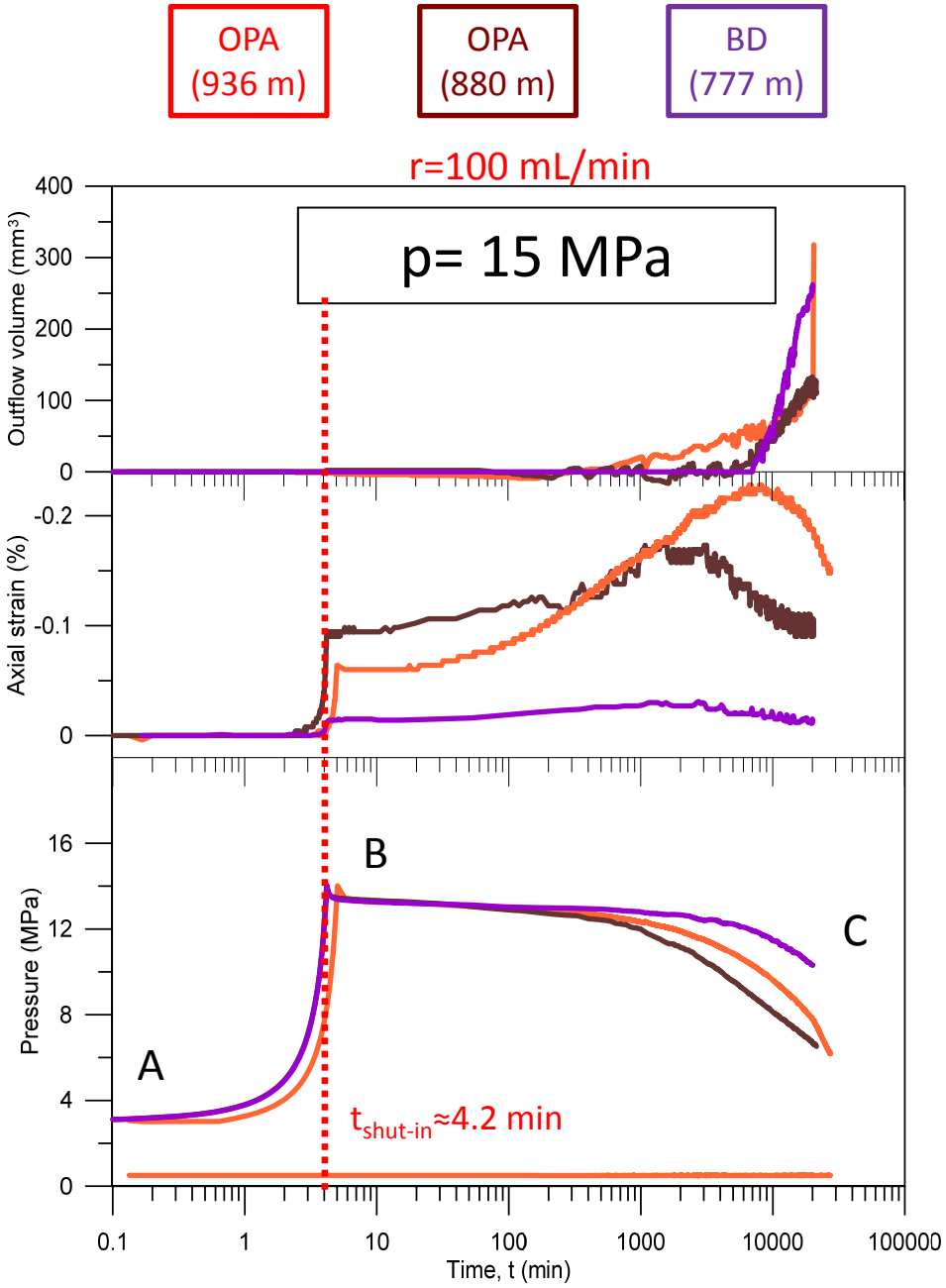

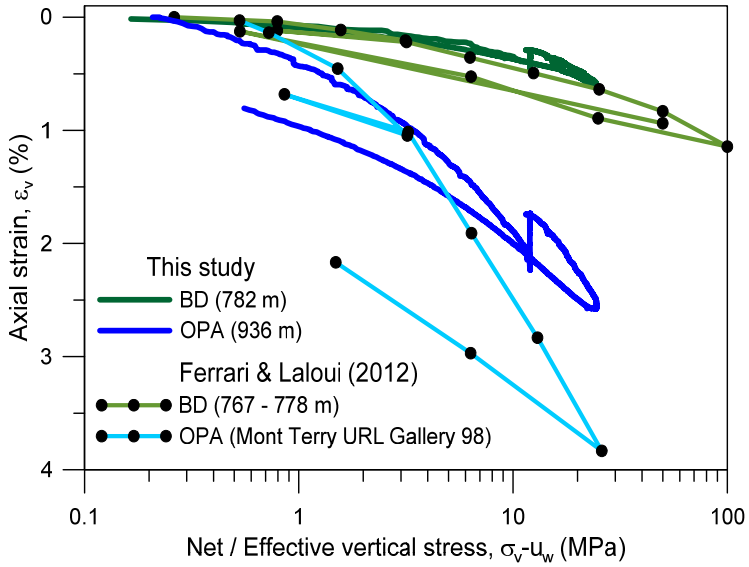

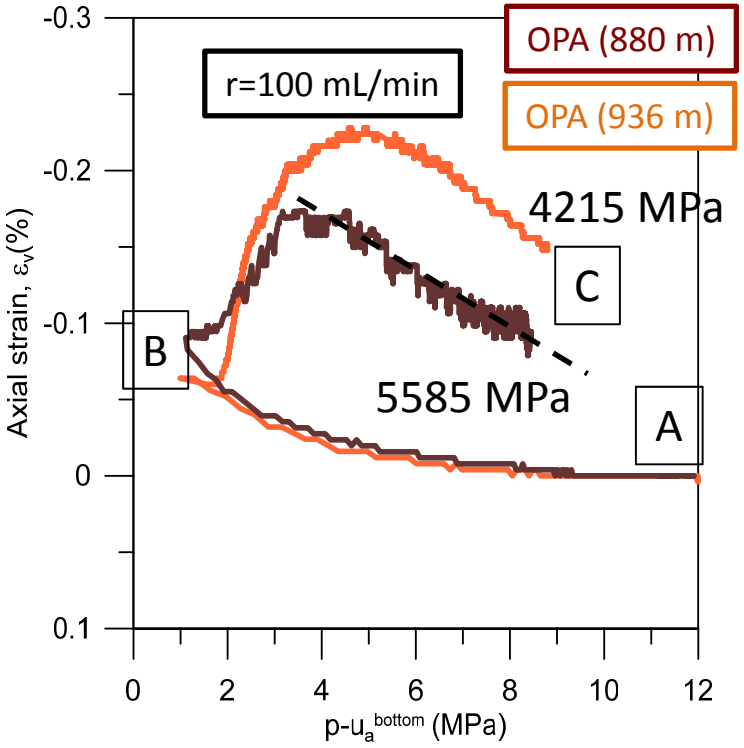

Air injection tests on BD: air injection rate effects. Below AEV

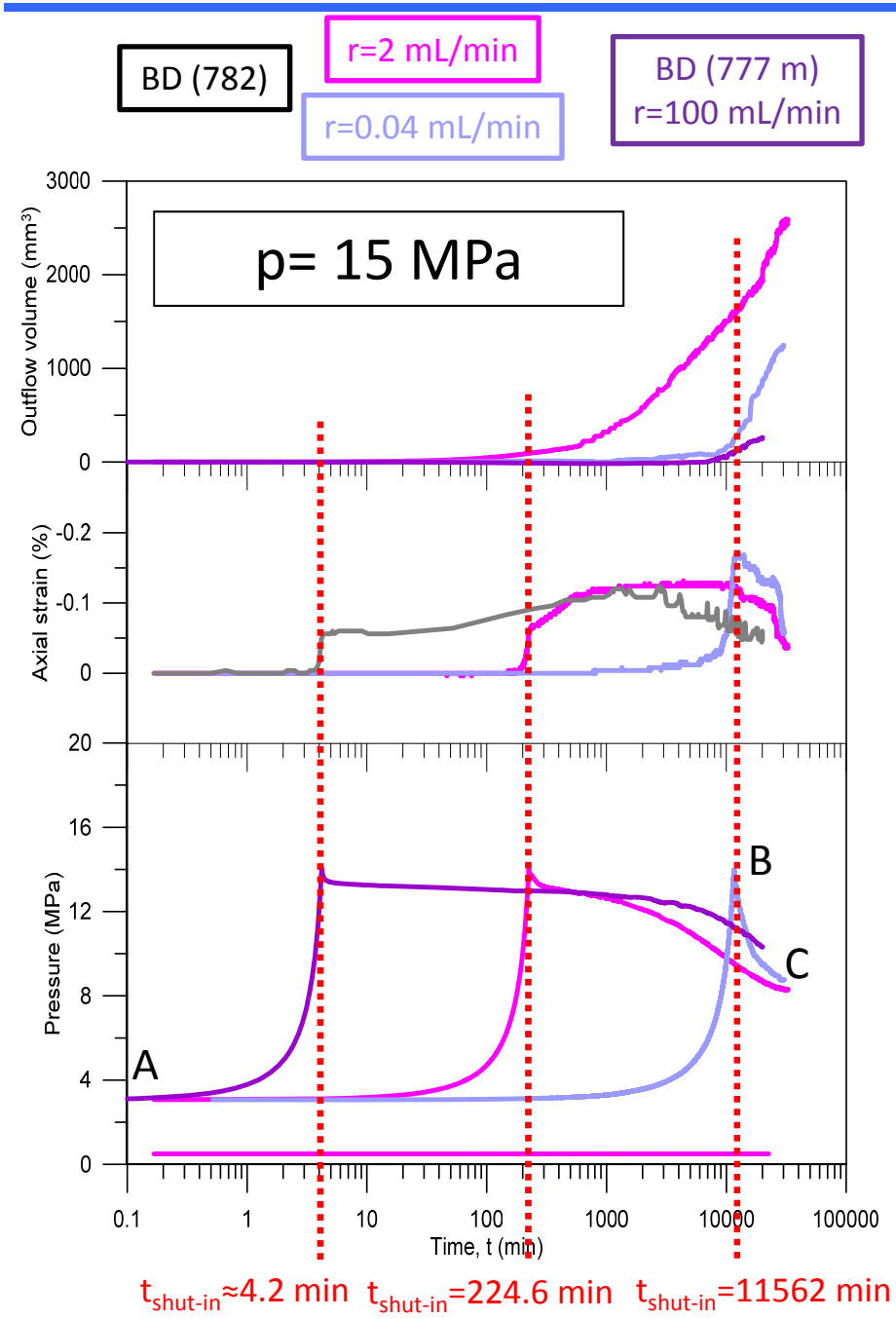

$t_{shut\text{-}in}$≈4.2 min $t_{shut\text{-}in}$=224.6 min $t_{shut\text{-}in}$=11562 min

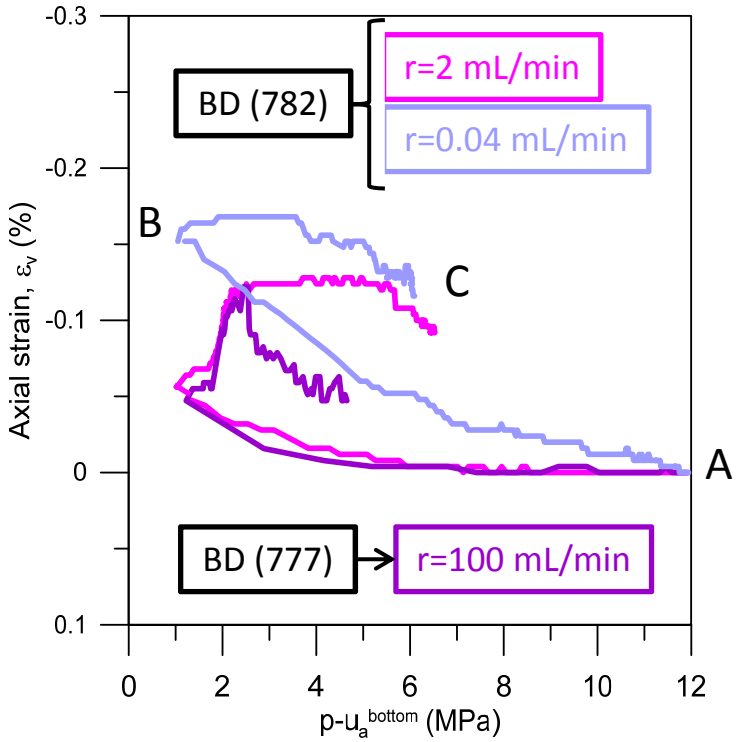

Slower injections (0.04 mL/min) induce higher expansions during the injection stage, while the pressure front propagated

Intrinsic permeability (air and water results)

Air permeability from injection pressure decay data

$$K = -\frac{2LV_{in}\mu_a}{A((p_{in}(t))^2 - (p_{out}(t))^2)}\frac{dp_{in}}{dt}$$

L: height of sample
A: sample area
μ_a: air viscosity
p_{in}: Injection pressure
p_{out}: pressure at recovery point
V_{in}: constant air injection volume

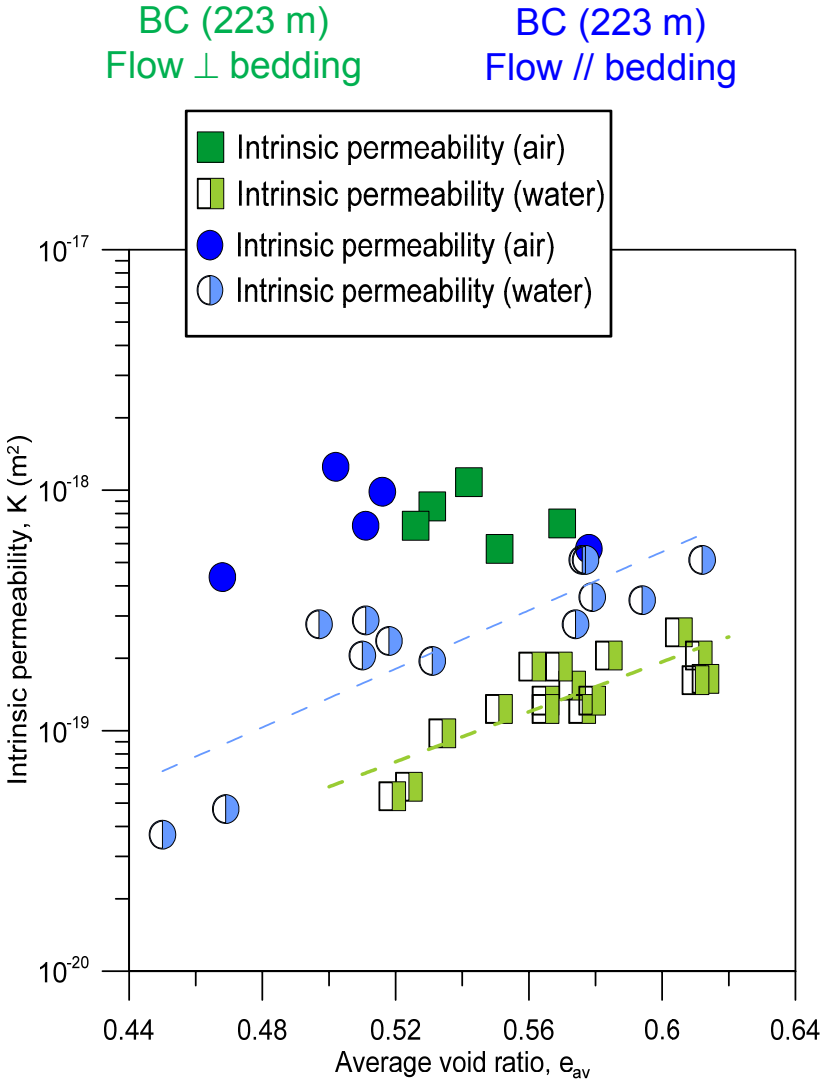

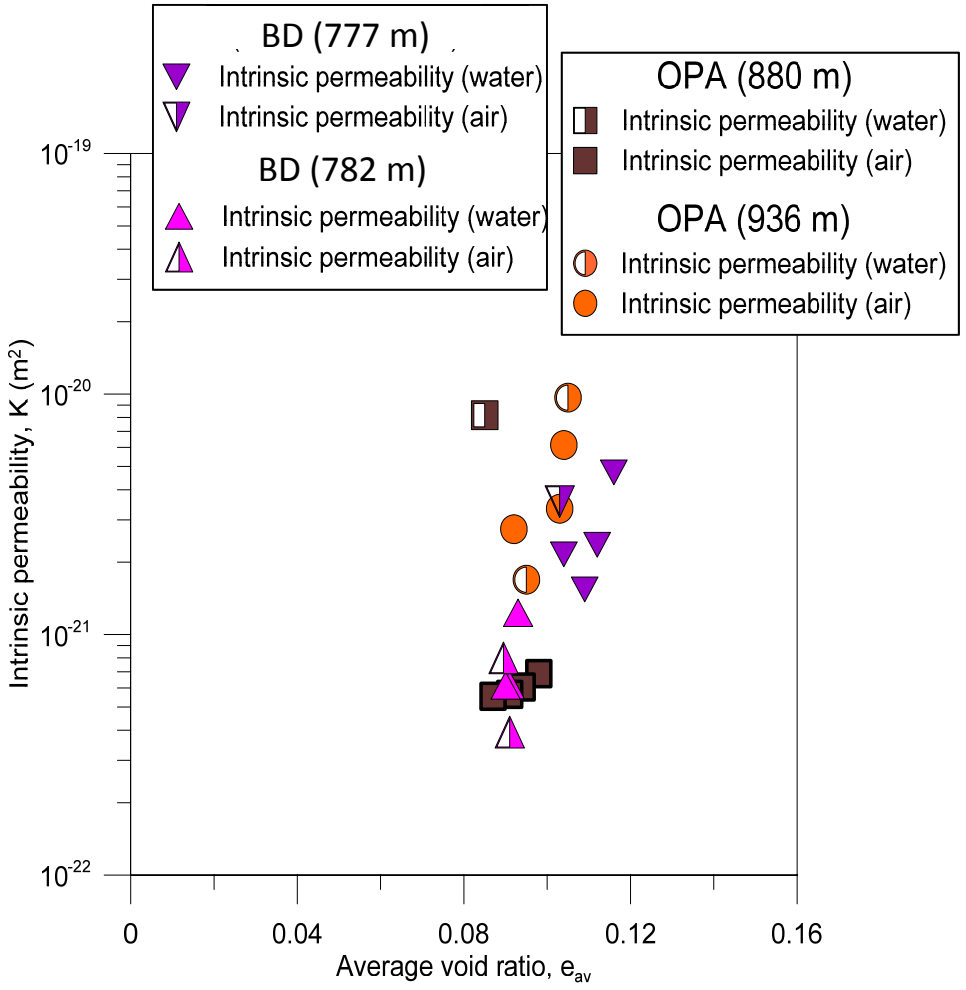

Two-phase flow code TOUGH2

OPA: Introducing coupled HM effects (based on experimental data), Grant model and Leverett function (capillary pressure with permeability)

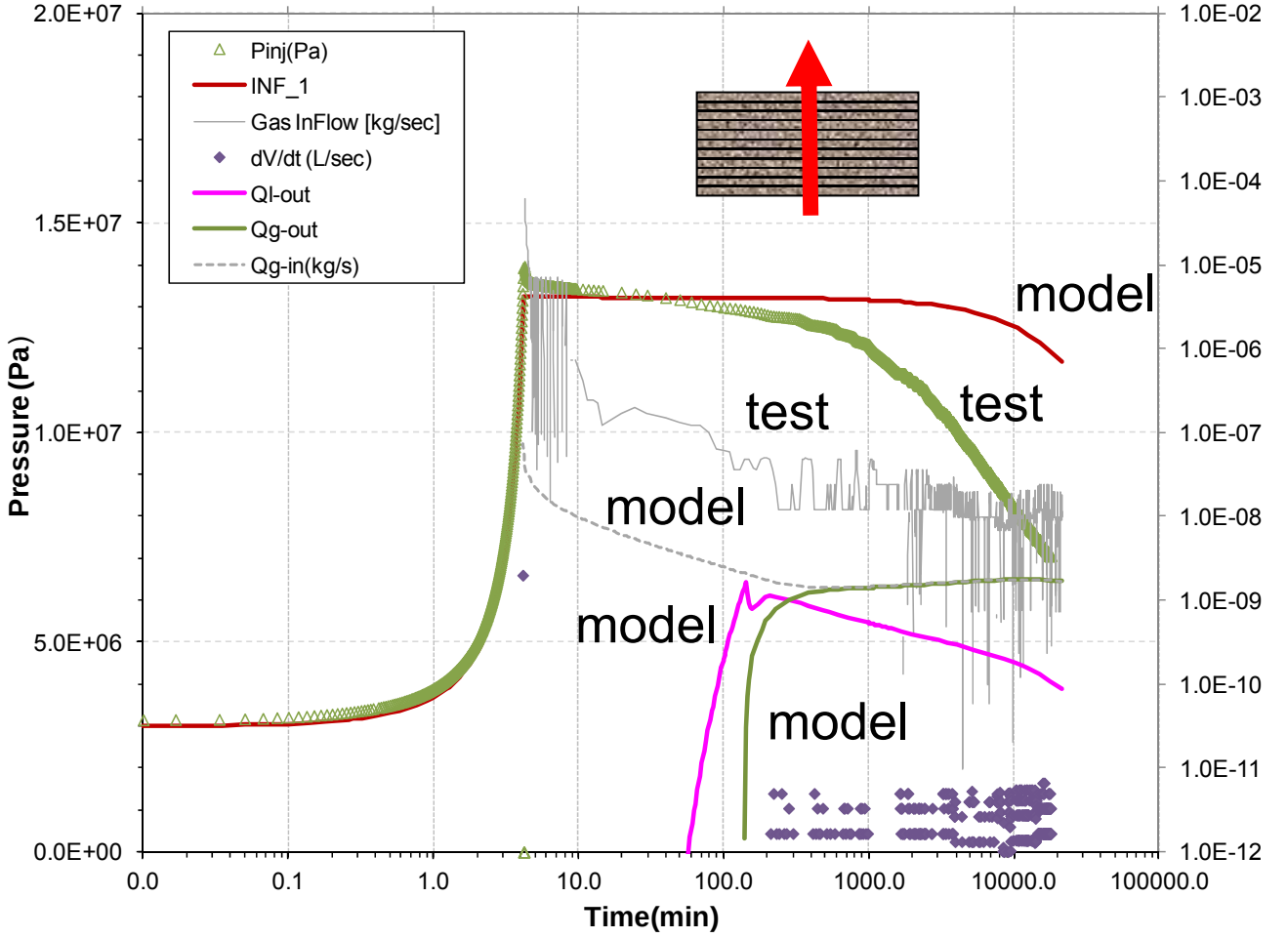

After air breakthrough:

$k_{rg} = 1 - k_{rl}$

Need to separate gas and liquid (outflow)

Tests difficult to interpret without the consideration of development of preferential paths. Need of constitutive relationships for pathway dilation

Senger et al. (2014)
Senger, Romero & Marschall (2015)

Revised analysis. Introducing coupled HM effects and Grant model

Senger, Romero, Ferrari, Marschall (2014)
Senger, Romero & Marschall (2015)

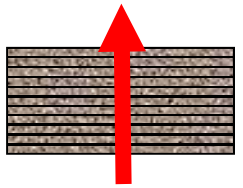

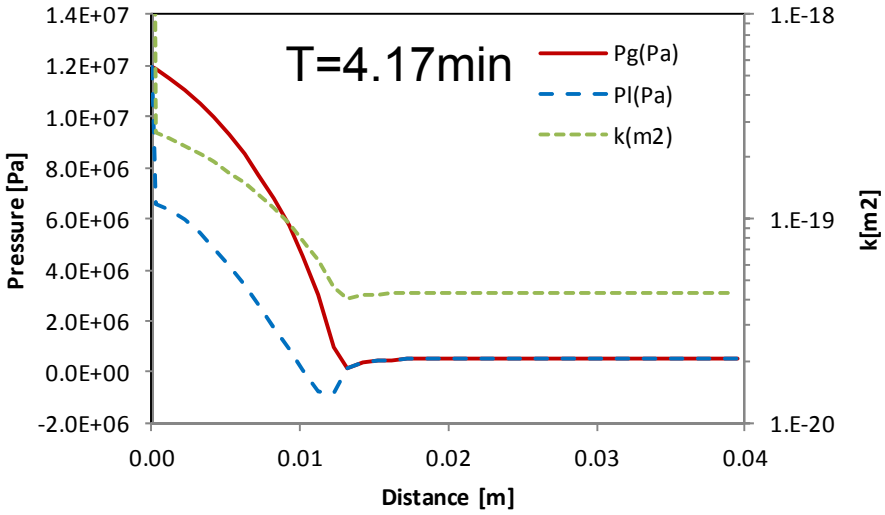

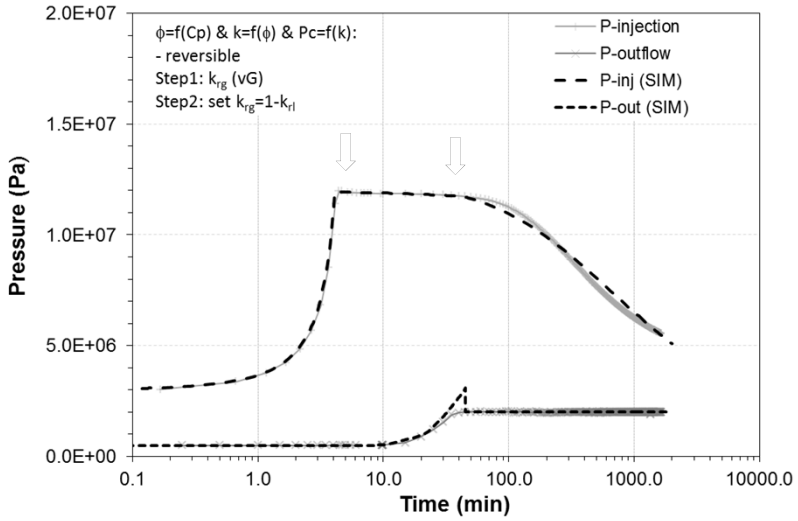

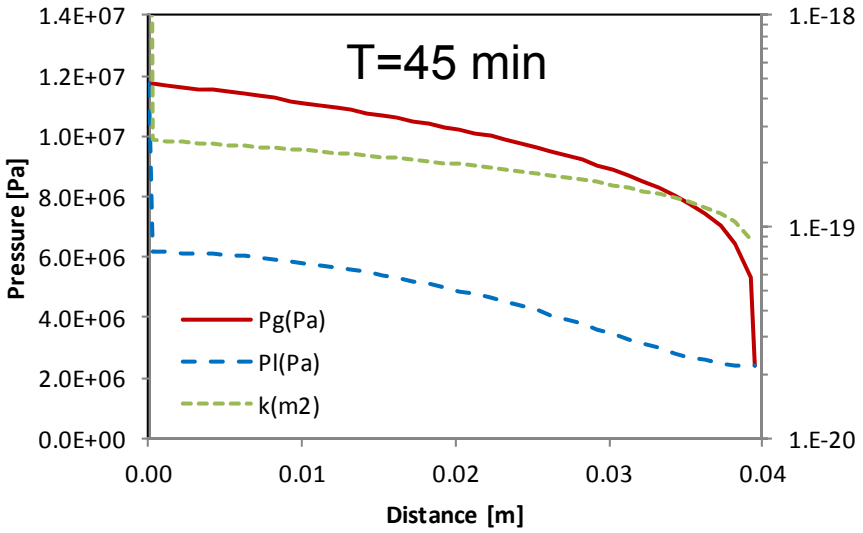

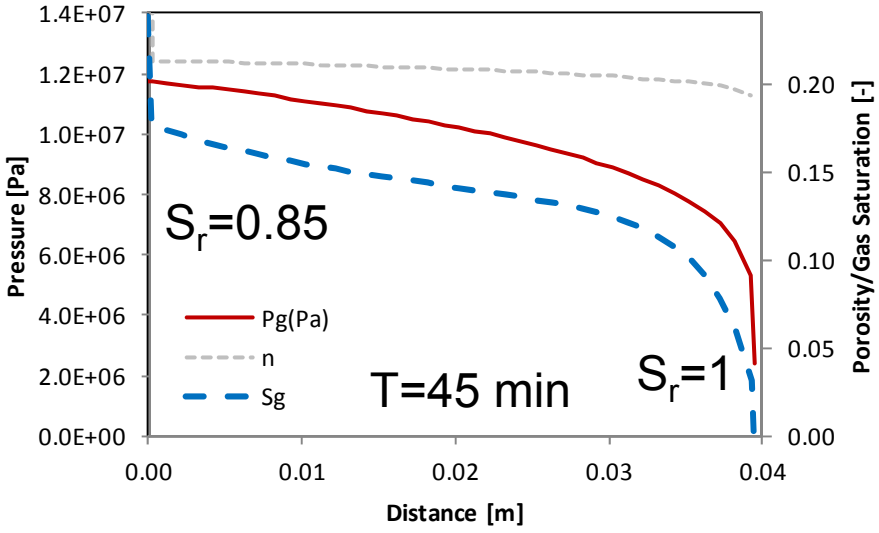

BC: Evolution of pore size distribution after air injection tests

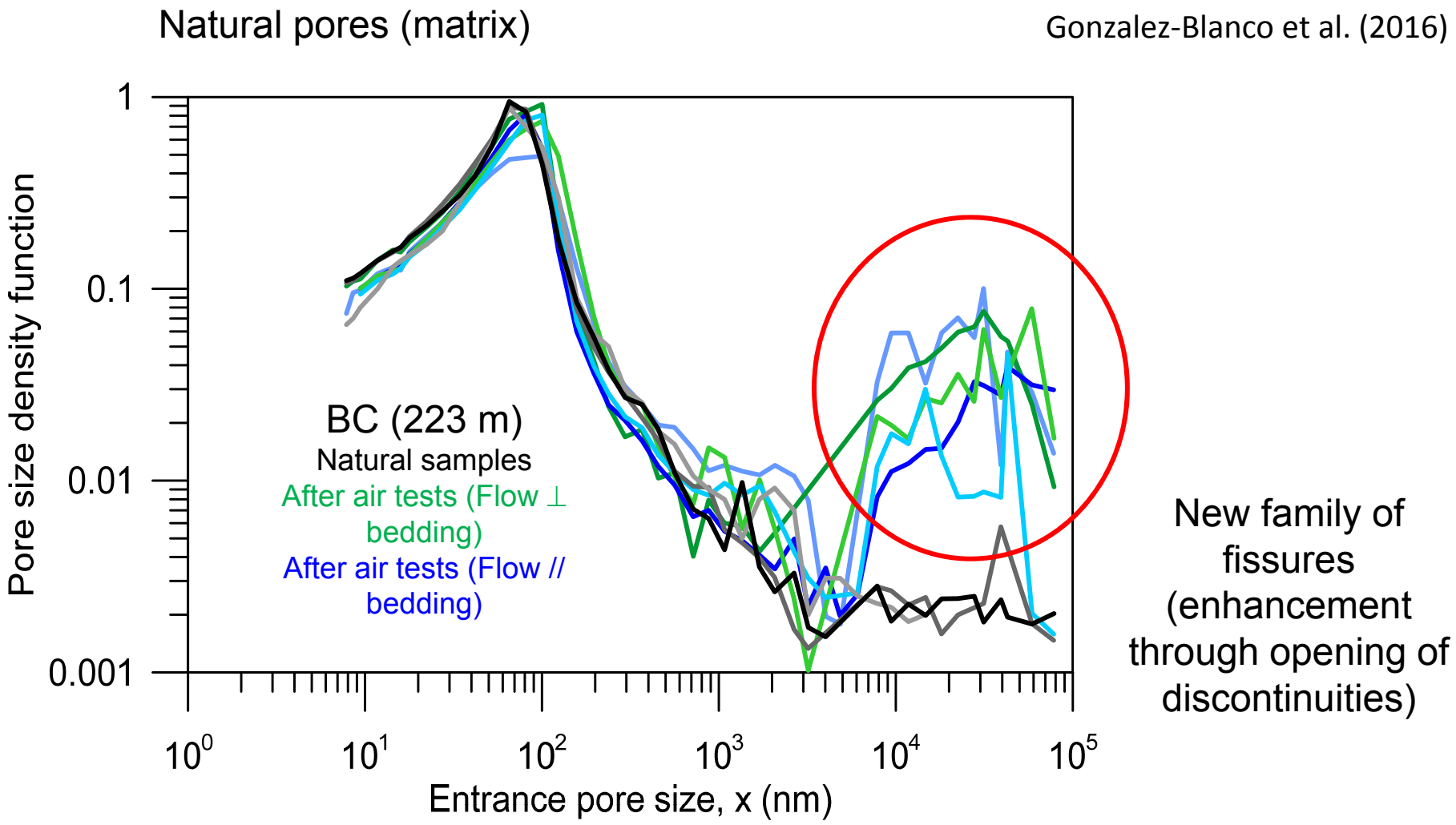

Bi-modal pore size distribution:
natural pores (matrix) and fissures (damage/degradation: dilatational pathways)

Micro-CT scan after air injection test (flow parallel to bedding planes)

Sample dimension:
Height ≈ 15 mm
Diameter ≈ 15 mm

Distance between slides = 0.02 mm

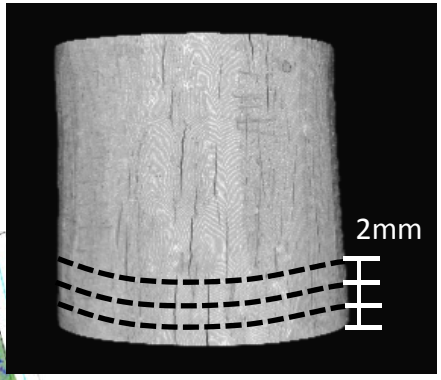

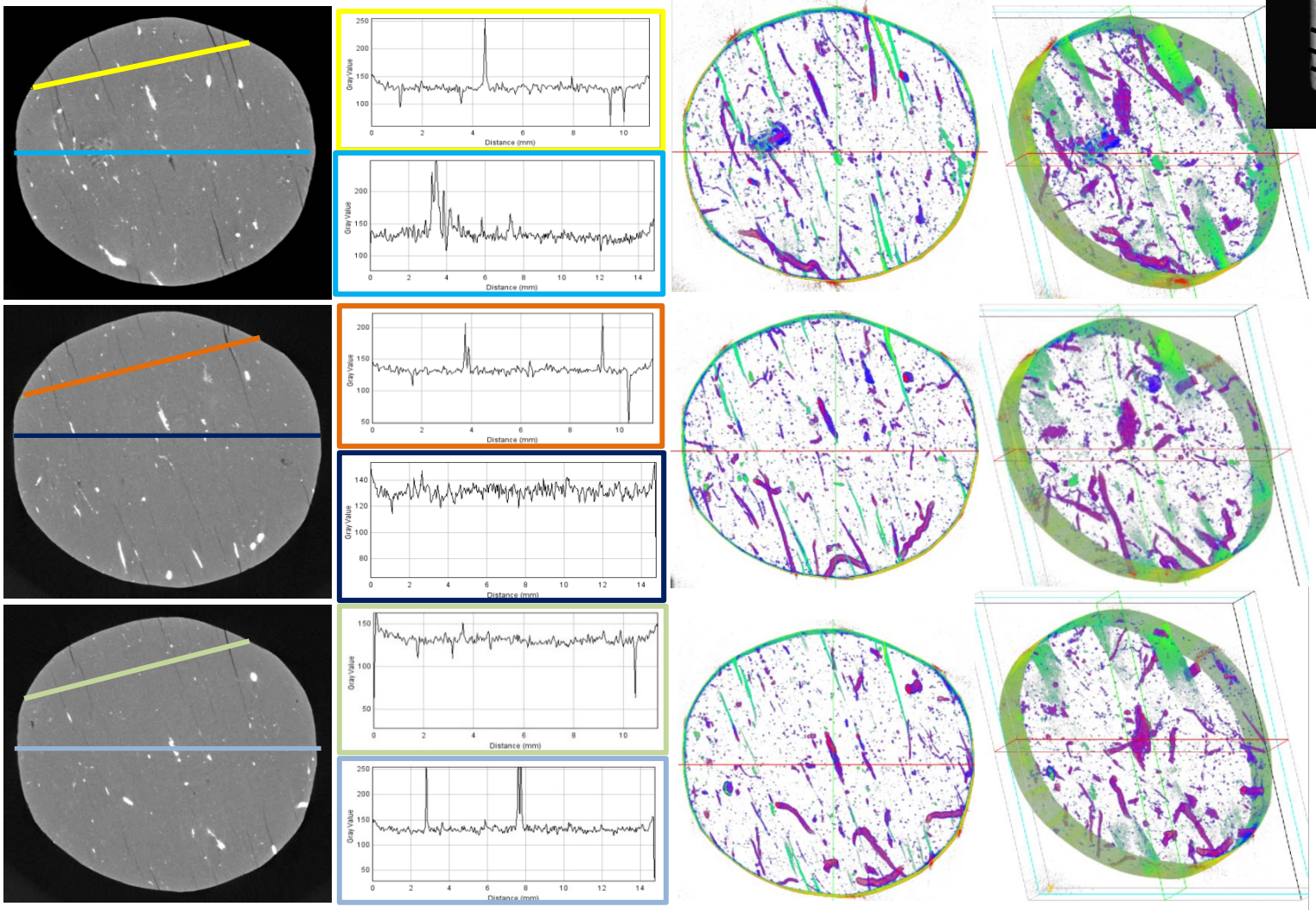

Bottom

Medium

Top

Fractal analysis of the pore size distribution (BC)

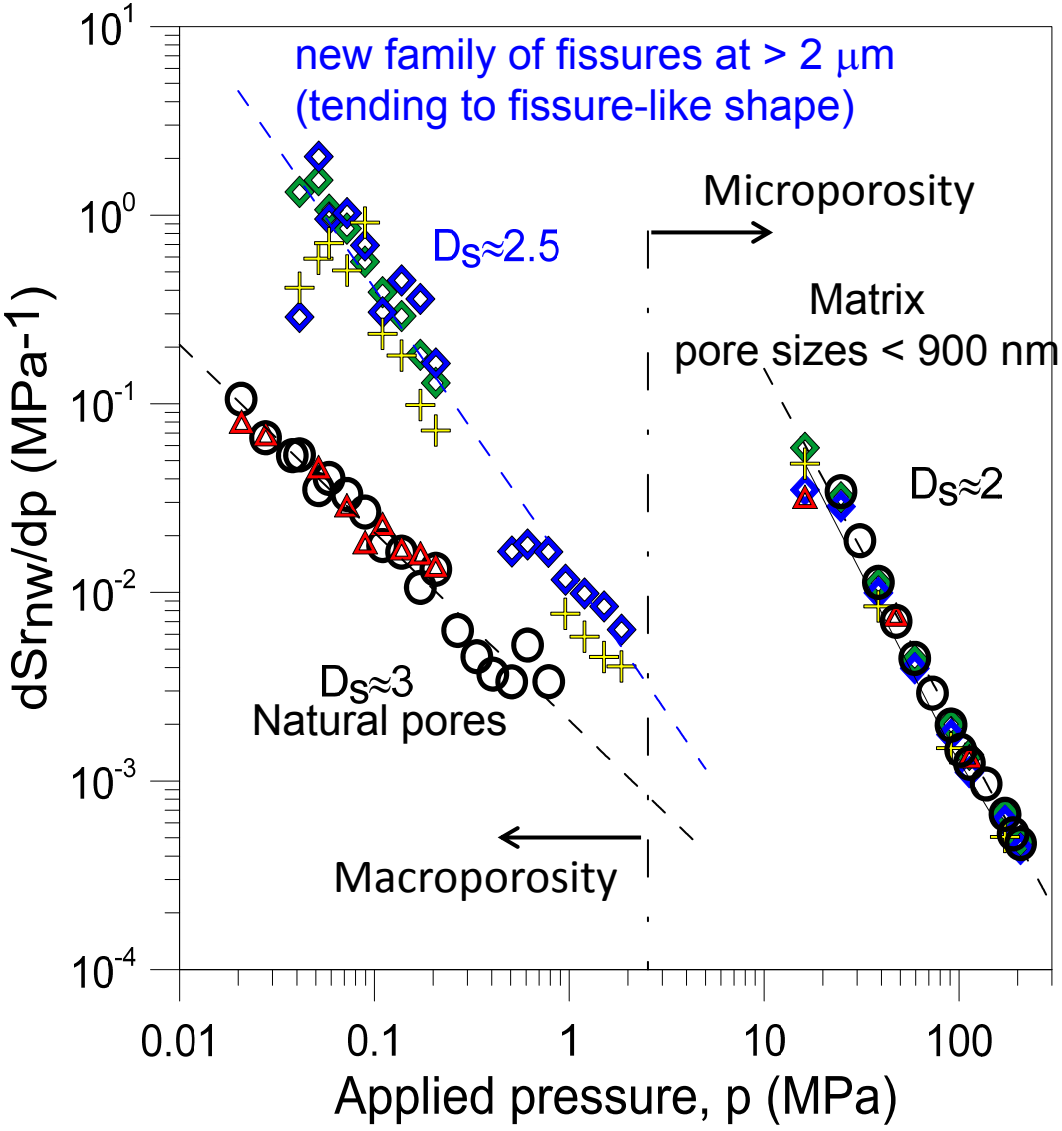

Fractal dimension: D_s

$$log\left(\frac{dSr_{nw}}{dp}\right) = -(D_s - 4)\log(p)$$

Intrinsic permeability (air and water) (BC)

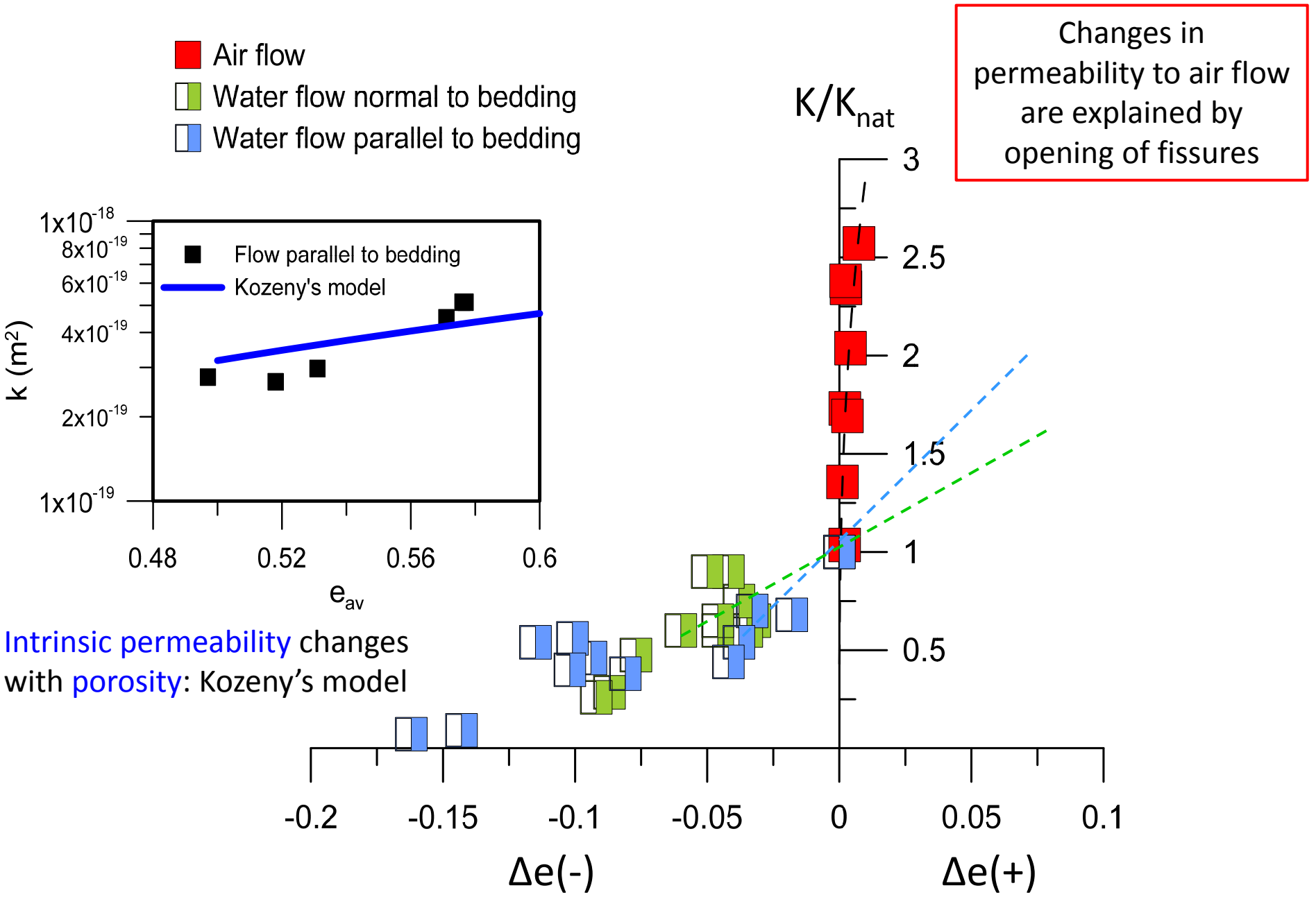

Intrinsic permeability (air) affected by fissure aperture

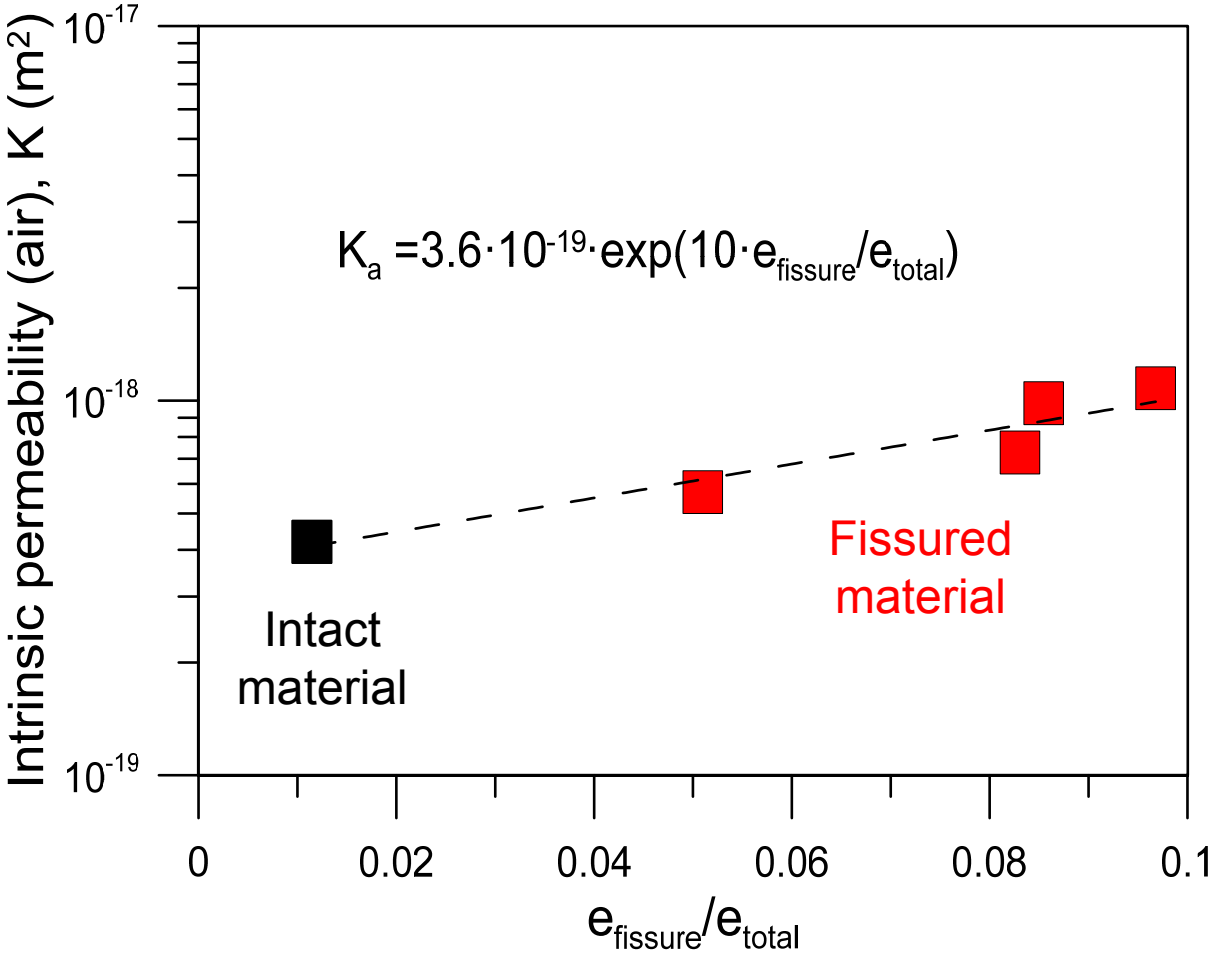

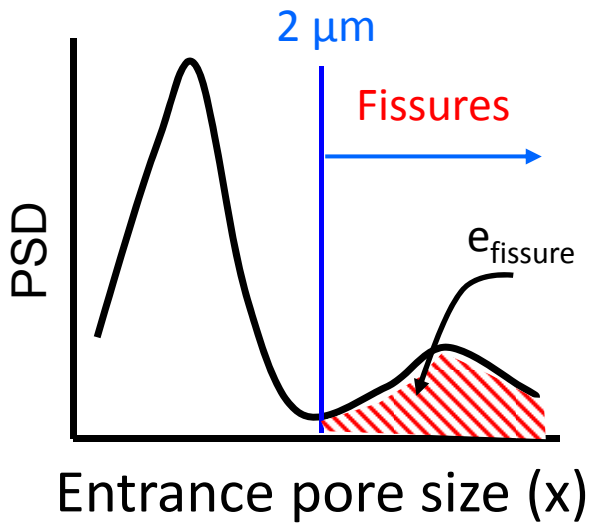

Fissure opening (BC)

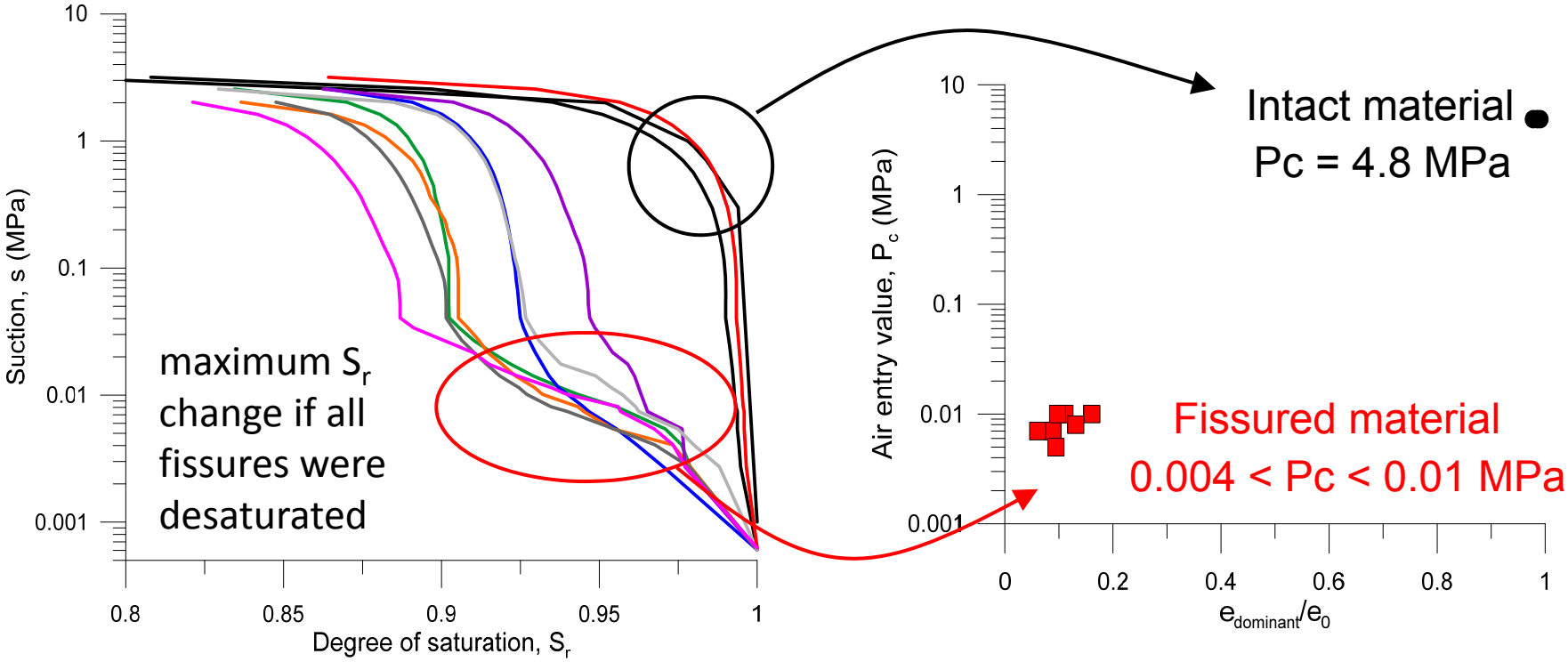

Desaturation of pathways is sometimes observed after sample dismantling

Bottom side OPA after injection test

Intrinsic permeability(enhancement through opening of embedded discontinuities)

a: fracture spacing
b: fracture aperture

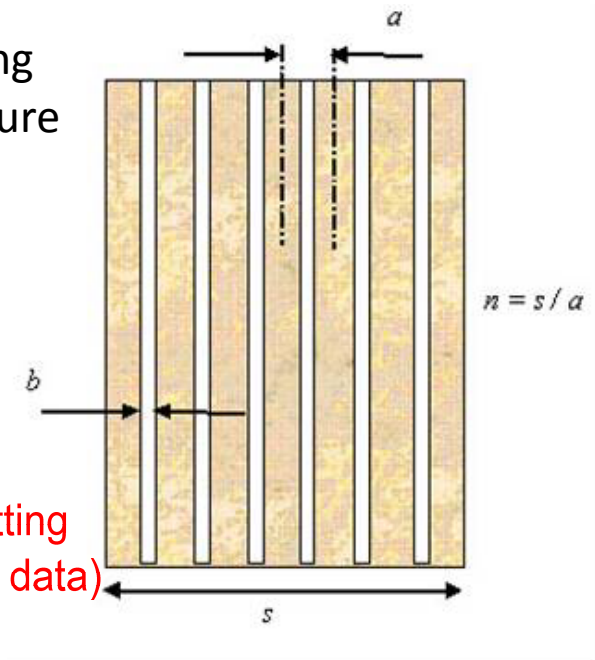

BC

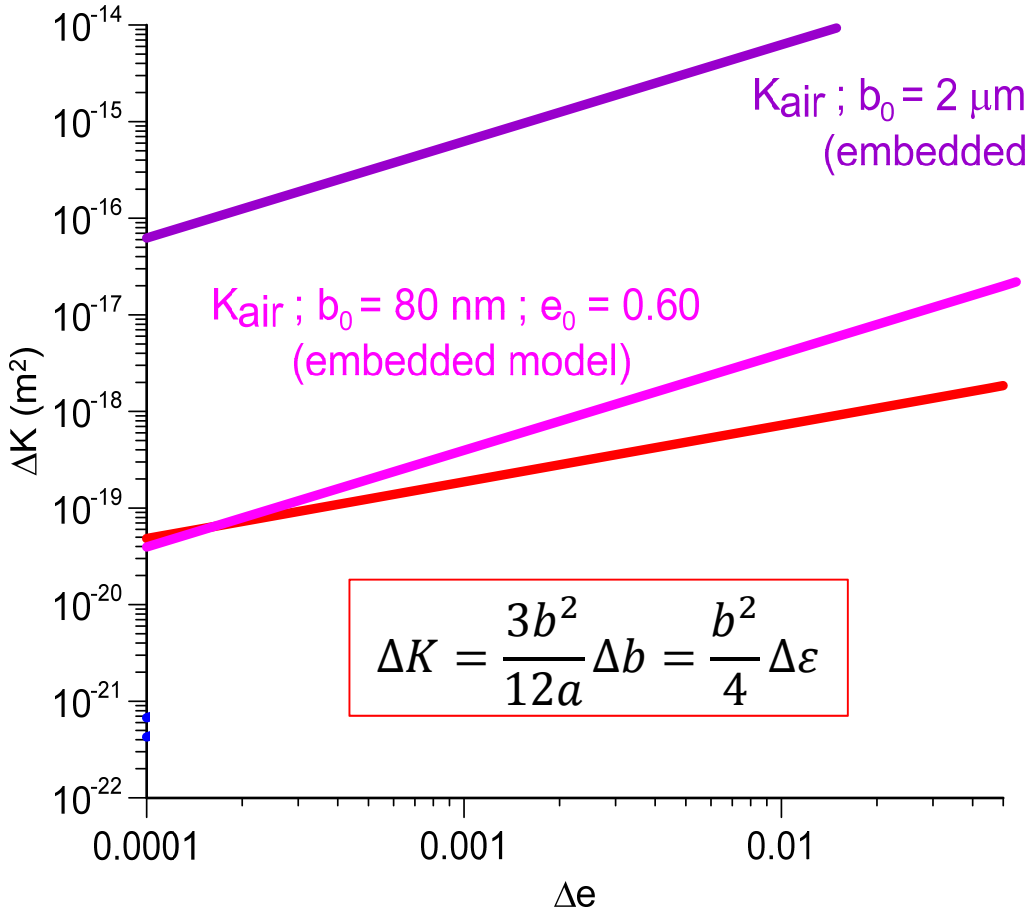

K_{air} ; b_0 = 2 μm ; e_0 = 0.60 (embedded model)

K_{air} ; b_0 = 80 nm ; e_0 = 0.60 (embedded model)

K_{air} (power fitting of experimental data)

$$\Delta K = \frac{3b^2}{12a}\Delta b = \frac{b^2}{4}\Delta\varepsilon$$

Enhancement through opening of embedded discontinuities in elements (Olivella & Alonso 2008)

Facture aperture variations

$$\Delta b = a\Delta\varepsilon = a(\varepsilon - \varepsilon_0) \text{ for } \varepsilon > \varepsilon_0$$

$$K_{fracture} = \frac{(b_0 + \Delta b)^2}{12}$$

Equivalent permeability

$$K = \frac{b^3}{12a}$$

Capillary pressure change (BC) (enhancement through opening of embedded discontinuities)

May explain changes in capillary pressure with very small changes in porosity

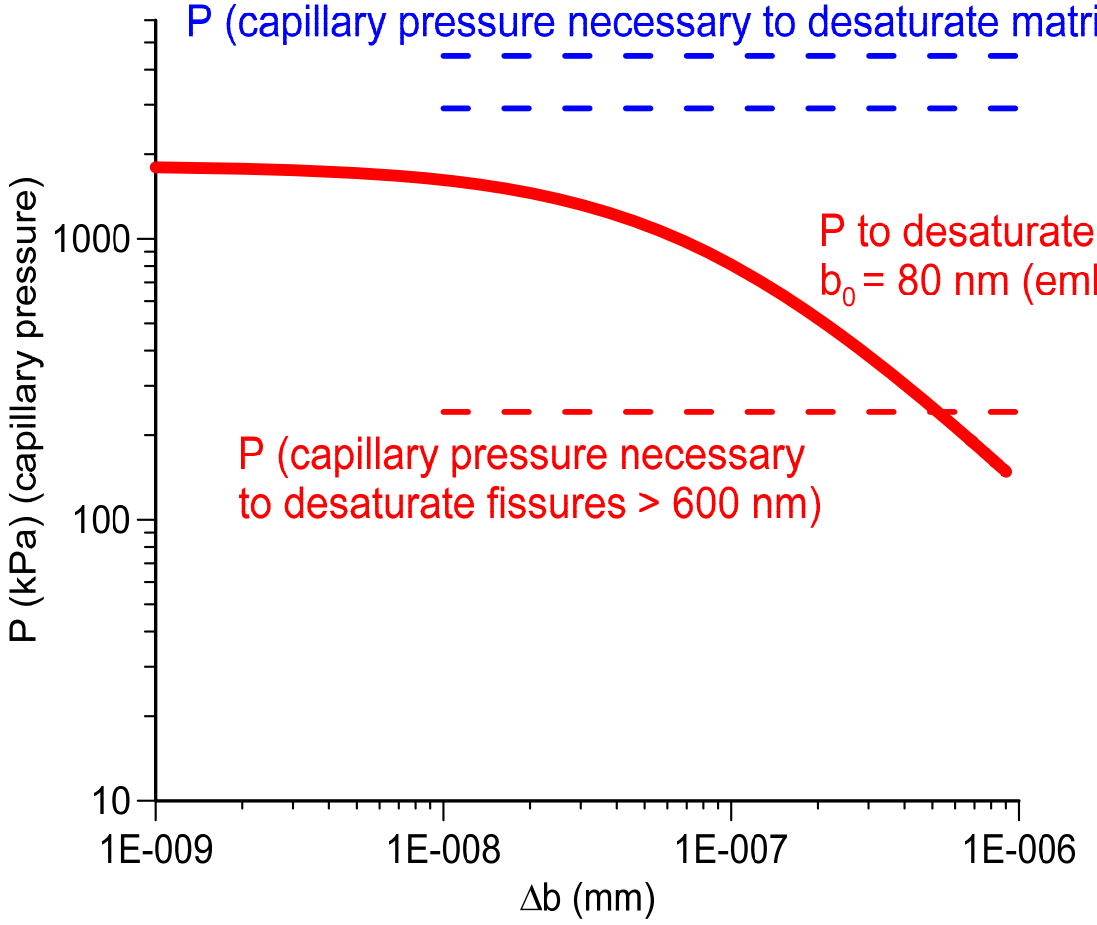

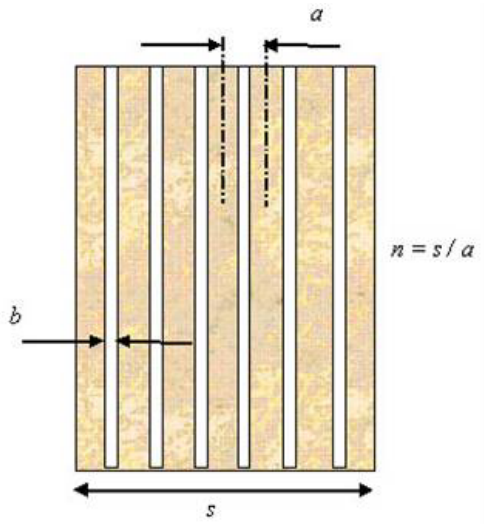

Facture aperture variations

$$\Delta b = a\Delta\varepsilon$$

$$P = \frac{2\sigma}{b} = \frac{2\sigma}{b_o}\left(\frac{b_o}{b}\right) = P_o \frac{\sqrt[3]{K_{fracture\_o}}}{\sqrt[3]{K_{fracture}}}$$

HM two-phase flow with embedded fracture permeability model (Code_Bright)

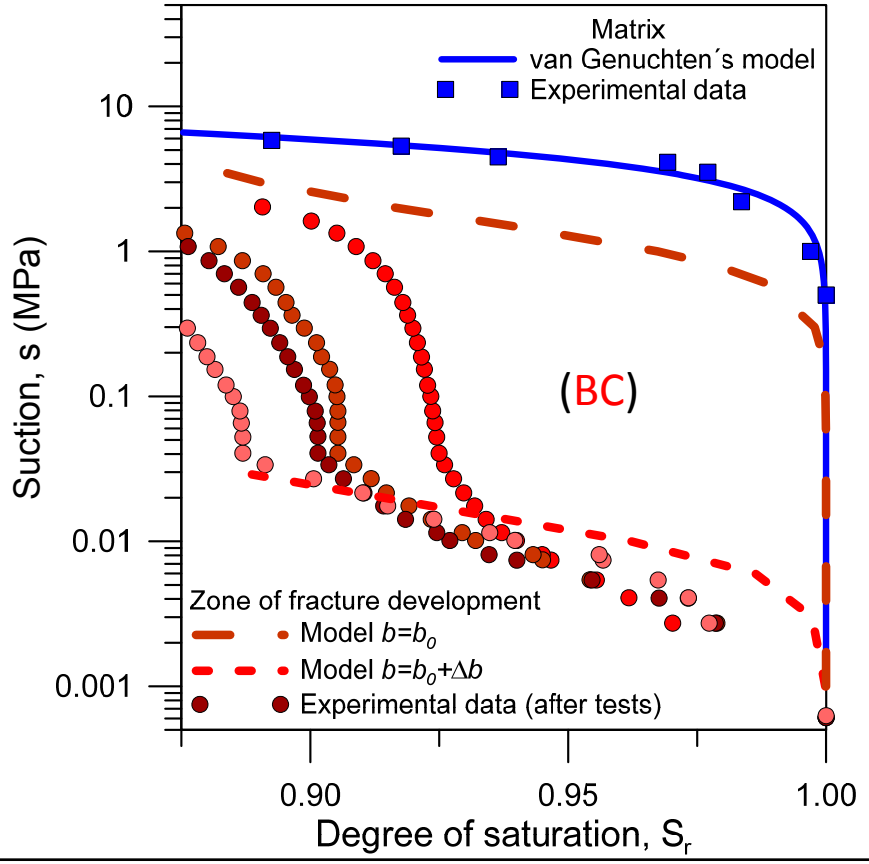

Embedded fracture permeability model		
Reference intrinsic permeability	k_0	$4.2 \cdot 10^{-19}$ m^2
Reference porosity	ϕ_0	0.363
Initial aperture	b_0	$1 \cdot 10^{-7}$ m
Threshold strain	ε_0	$-1 \cdot 10^{-6}$
Maximum aperture	b_{max}	$3 \cdot 10^{-6}$ m
Characteristic dimension	a	$3 \cdot 10^{-5}$ m

Gonzalez-Blanco et al. (2016)

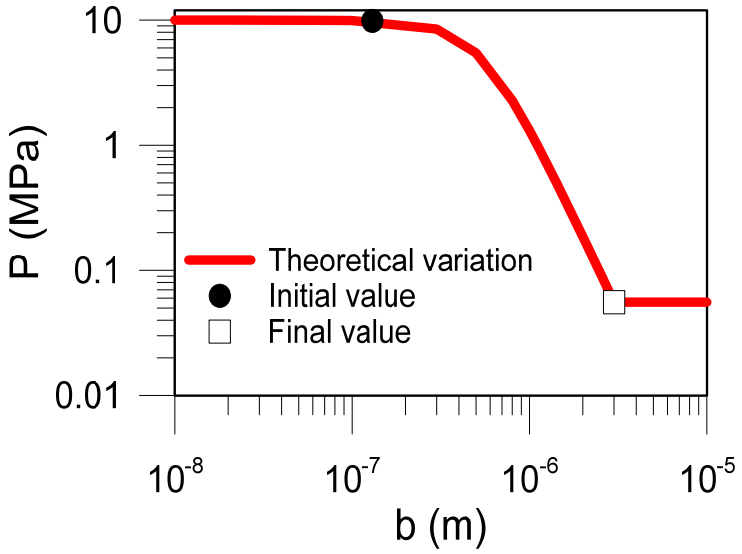

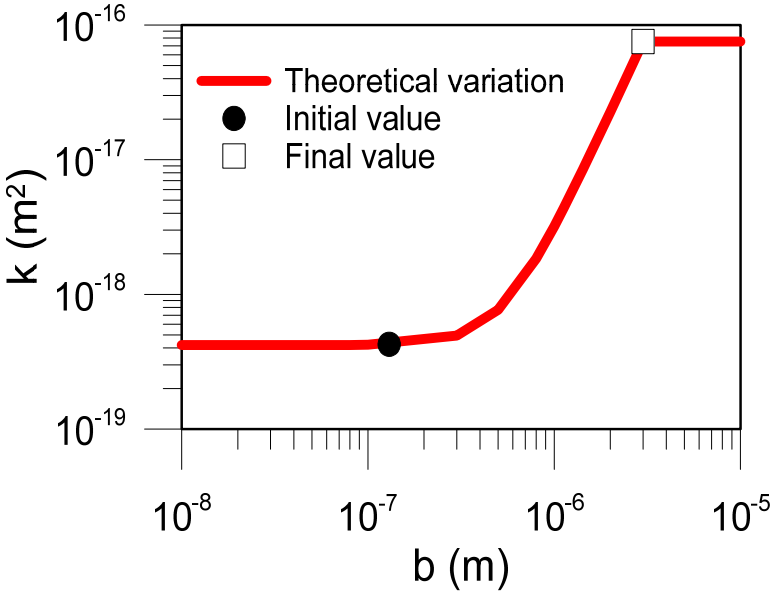

Existing fractures ($\sigma_t = 0$) and initially open ($\varepsilon_0 < 0$)

Materials and boundary conditions for numerical simulation

To achieve suitable results, it is necessary to take into account the volume of the upstream and downstream reservoirs of the experimental set-up in the simulation

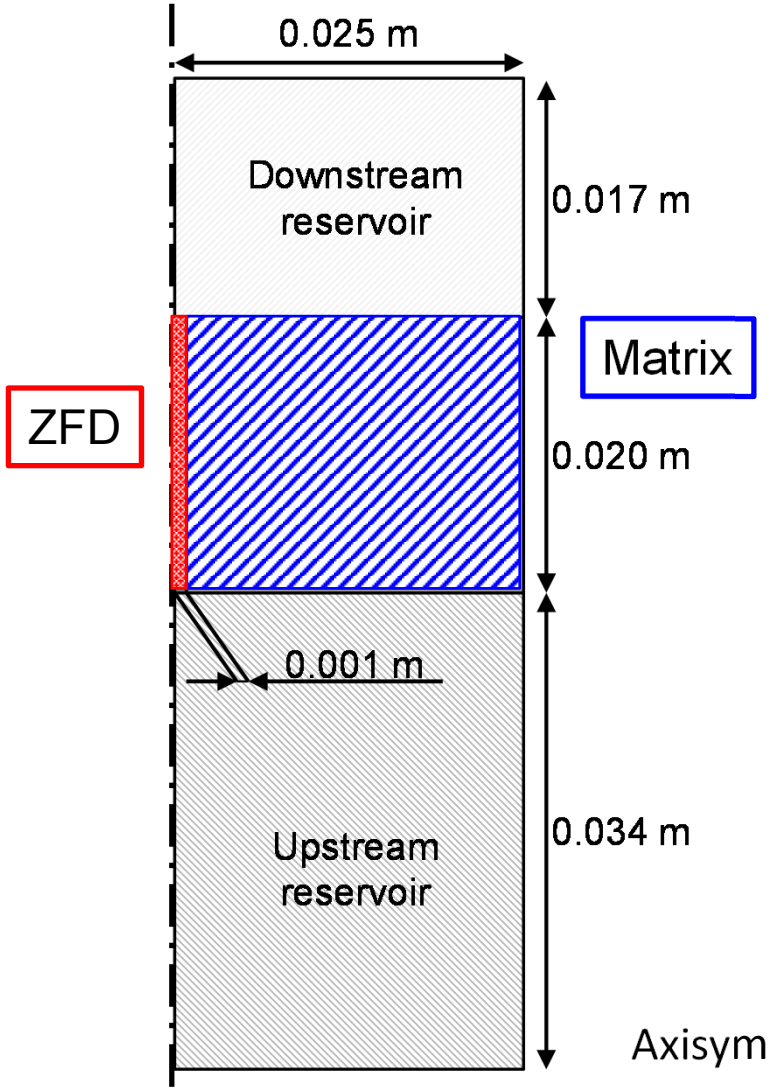

Axisymmetric geometry

Air flow at constant volume injection rate (2 mL/min) was imposed at the bottom boundary through an air injection pressure ramp

Air flow at the injection point present comparable results

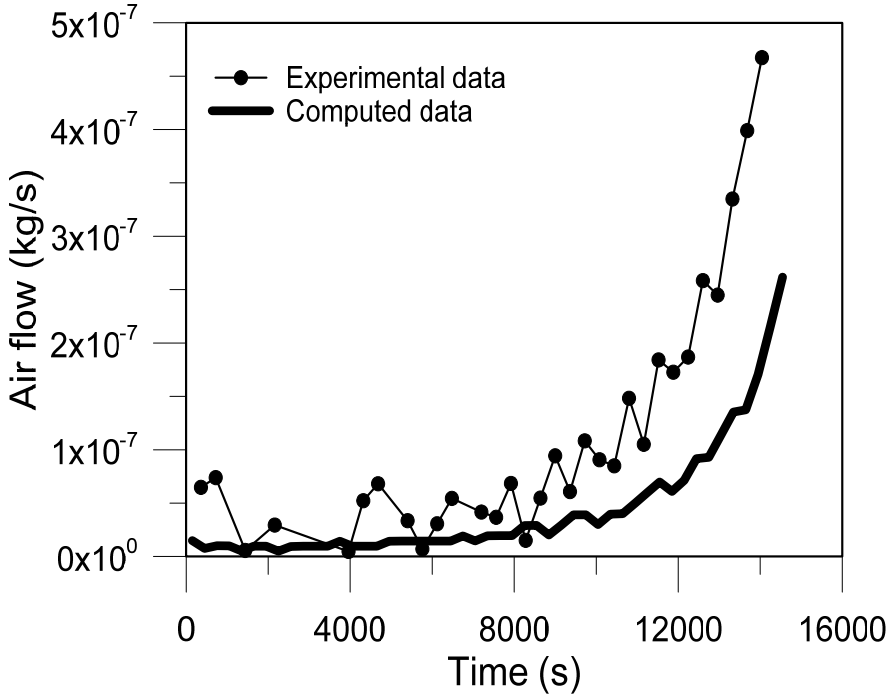

Gonzalez-Blanco et al. (2016)

Experimental vs. simulated results of slow air injection test (BC)

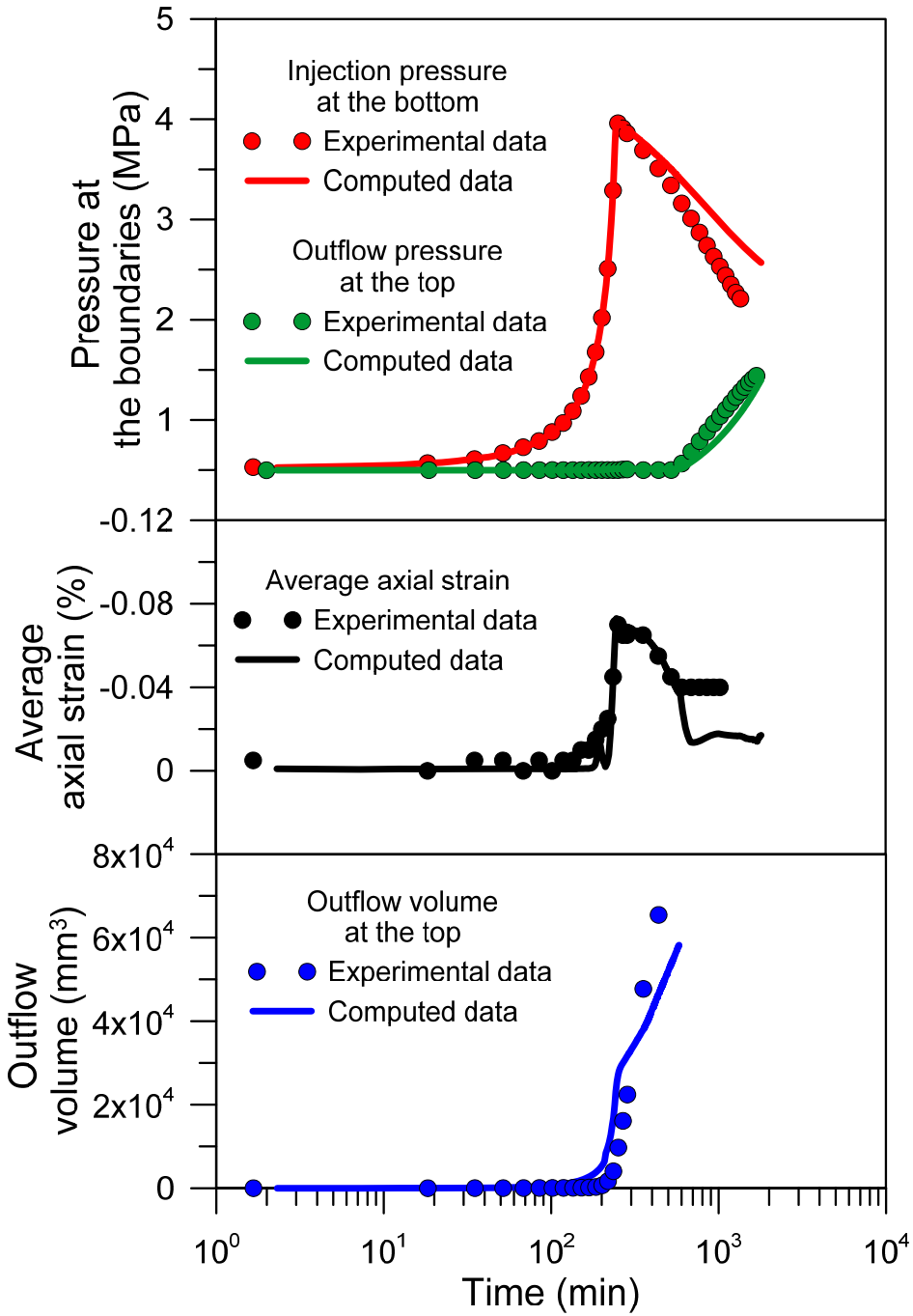

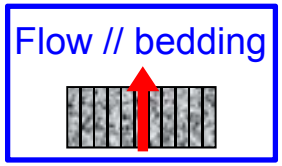

2 mL/min

L. Gonzalez-Blanco, E. Romero, C. Jommi, X. Li, X. Sillen (2016). Geomechanics for Energy and the Environment. Doi: 10.1016/j.gete.2016.04.002

Evolution of gas pressure, porosity and degree of saturation during air injection and dissipation (BC)

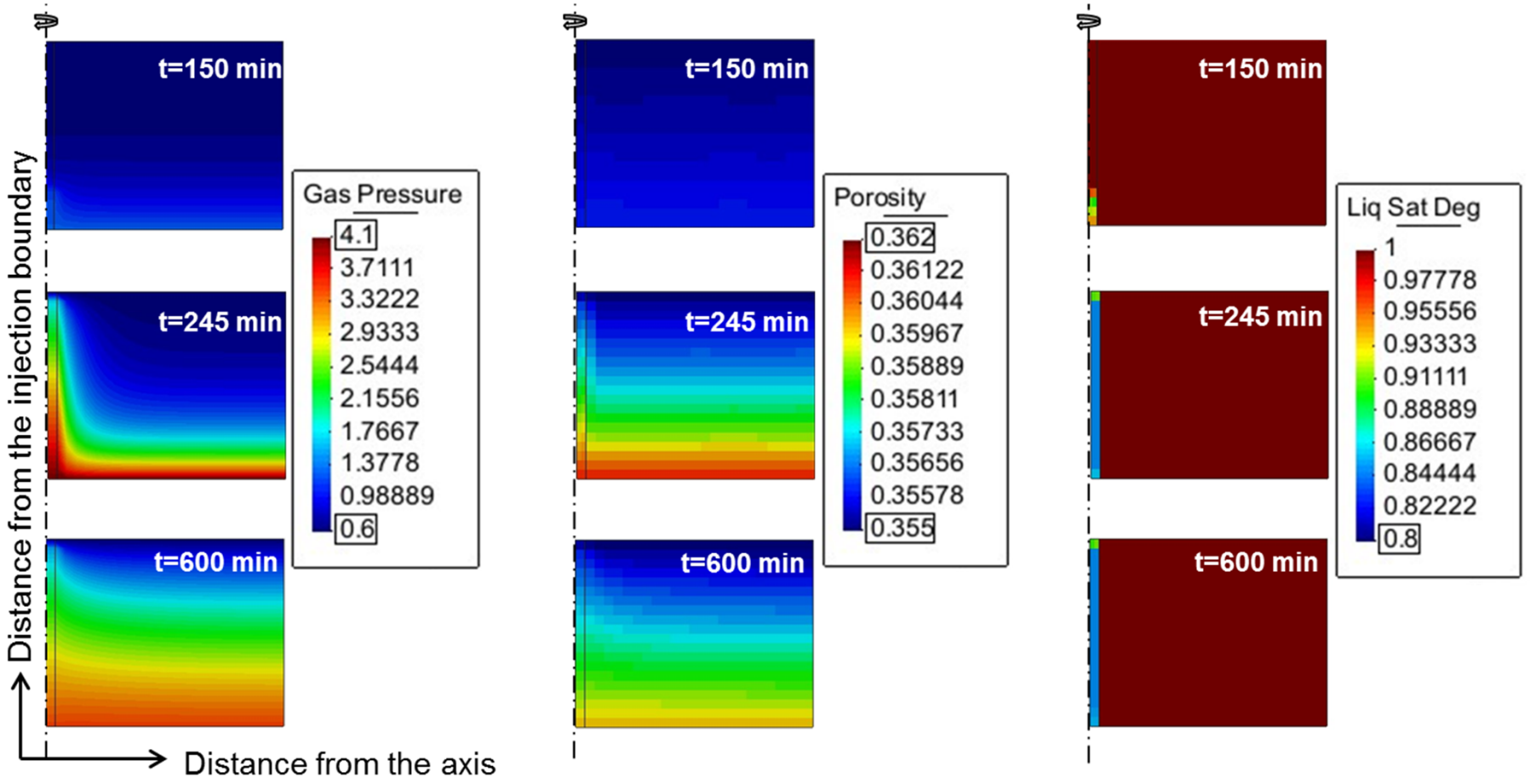

t= 150 min → During gas injection
t= 245 min → At shut-off (end of the injection)
t= 600 min → During gas dissipation

L. Gonzalez-Blanco, E. Romero, C. Jommi, X. Li, X. Sillen (2016). Geomechanics for Energy and the Environment. Doi: 10.1016/j.gete.2016.04.002

Computed local radial strains and radial displacements

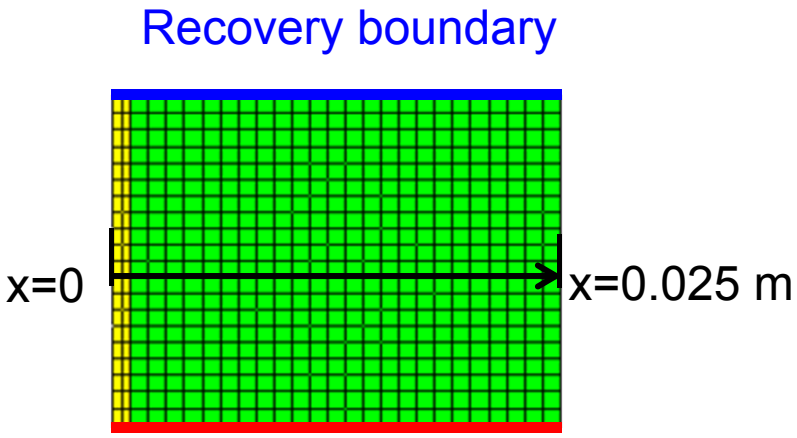

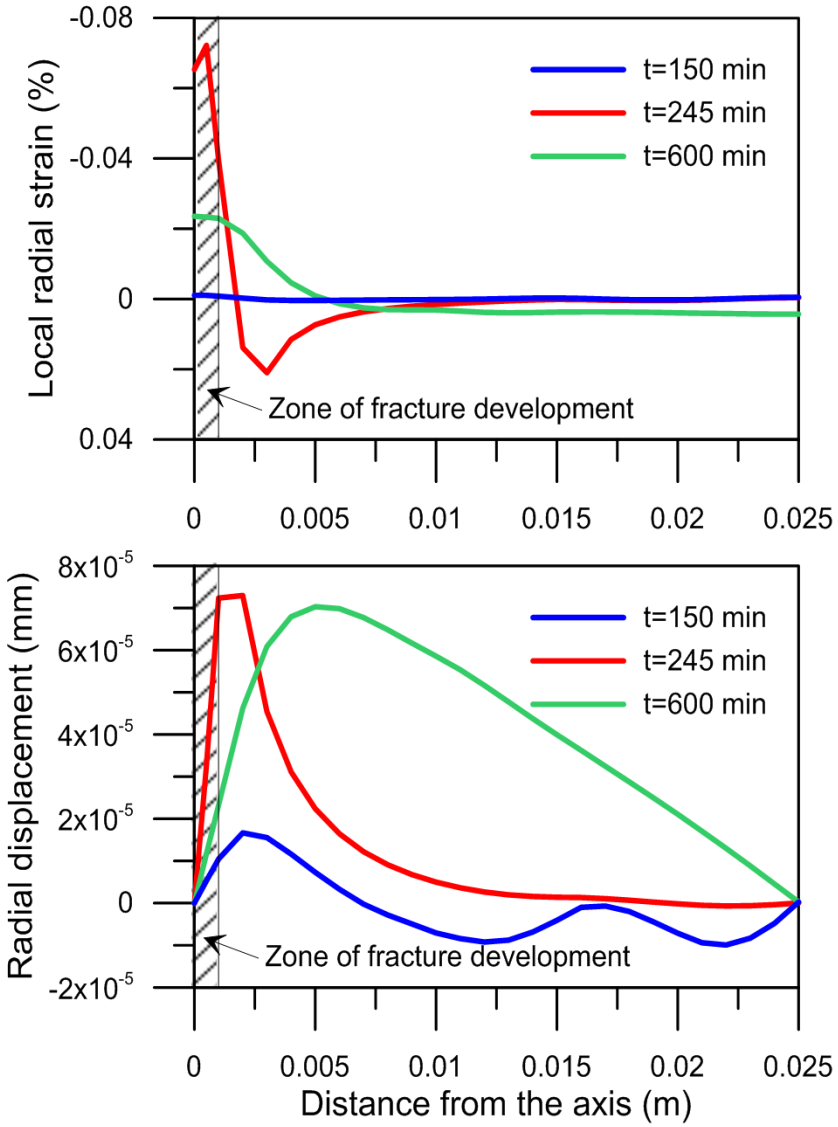

t= 150 min → During gas injection
t= 245 min → At shut-off (end of the injection)
t= 600 min → During gas dissipation

L. Gonzalez-Blanco, E. Romero, C. Jommi, X. Li, X. Sillen (2016). Geomechanics for Energy and the Environment. Doi: 10.1016/j.gete.2016.04.002

Computed advective and diffusive gas fluxes

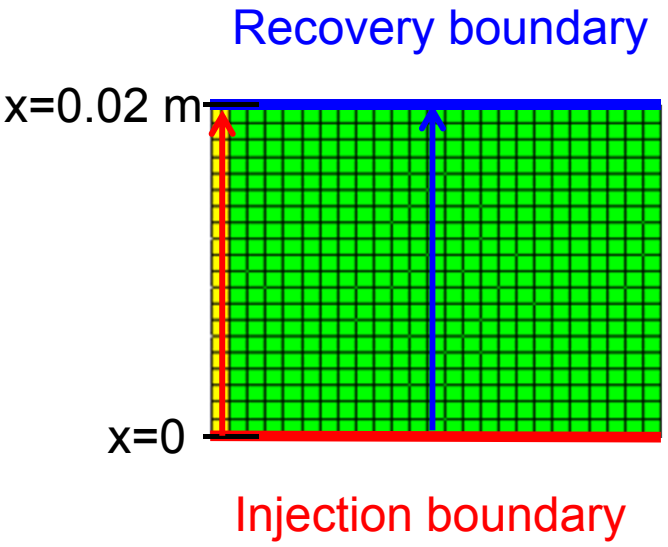

t= 150 min → During gas injection
t= 245 min → At shut-off (end of the injection)
t= 600 min → During gas dissipation

Need to separate
gas and liquid
(outflow)

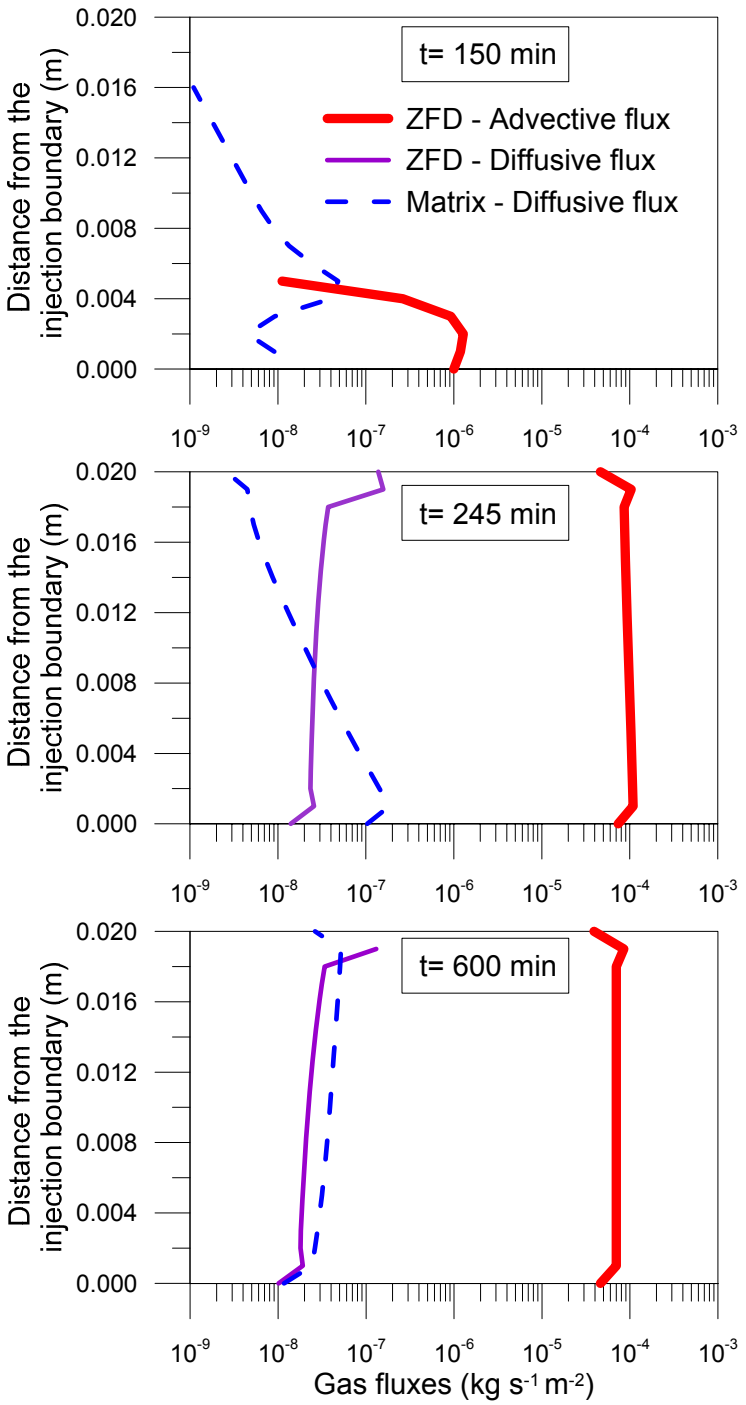

L. Gonzalez-Blanco, E. Romero, C. Jommi, X. Li, X. Sillen (2016). Geomechanics for Energy and the Environment. Doi: 10.1016/j.gete.2016.04.002

Summary and concluding remarks

❑ Controlled volume-rate air injection followed by dissipation stages have been presented (air injection rates, medium and deep clay formations) and focused on the **volume change response** and the **changes in the pore network (opening of fissures)**

❑ Microstructural changes (fissure-like opening at entrance pore sizes > 2μm) were found after injection tests. Opening of fissures appears to play an important role on air transport properties (intrinsic permeability and air-entry value)

❑ Need for coupled HM effects (compressibility of the material and changes in porosity along the sample) and higher air mobility (constitutive relationships for pathway dilation)

❑ The overall response of the gas migration process was reproduced using HM coupled models with embedded pressure-dependent fractures. The model handles the combined phenomena of two-phase flow (air and liquid) and the aperture of discrete paths to account for permeability and capillary pressure variations

Acknowledgements

The authors acknowledge the financial support provided by NAGRA (Switzerland) and ONDRAF / NIRAS (Belgium) through different research projects with International Center for Numerical Methods in Engineering (Spain). Thanks are also expressed to Prof. C. Jommi